© 2017. Published by The Company of Biologists Ltd | Journal of Cell Science (2017) 130, 3713-3727 doi:10.1242/jcs.206318

RESEARCH ARTICLE

Distinct intracellular sAC-cAMP domains regulate ER Ca^{2+} signaling and OXPHOS function

Federica Valsecchi[1], Csaba Konrad[1], Marilena D'Aurelio[1], Lavoisier S. Ramos-Espiritu[2,3], Anna Stepanova[1], Suzanne R. Burstein[1], Alexander Galkin[1], Jordi Magranè[1], Anatoly Starkov[1], Jochen Buck[2], Lonny R. Levin[2] and Giovanni Manfredi[1,*]

ABSTRACT

cAMP regulates a wide variety of physiological functions in mammals. This single second messenger can regulate multiple, seemingly disparate functions within independently regulated cell compartments. We have previously identified one such compartment inside the matrix of the mitochondria, where soluble adenylyl cyclase (sAC) regulates oxidative phosphorylation (OXPHOS). We now show that sAC knockout fibroblasts have a defect in OXPHOS activity and attempt to compensate for this defect by increasing OXPHOS proteins. Importantly, sAC knockout cells also exhibit decreased probability of endoplasmic reticulum (ER) Ca^{2+} release associated with diminished phosphorylation of the inositol 3-phosphate receptor. Restoring sAC expression exclusively in the mitochondrial matrix rescues OXPHOS activity and reduces mitochondrial biogenesis, indicating that these phenotypes are regulated by intramitochondrial sAC. In contrast, Ca^{2+} release from the ER is only rescued when sAC expression is restored throughout the cell. Thus, we show that functionally distinct, sAC-defined, intracellular cAMP signaling domains regulate metabolism and Ca^{2+} signaling.

KEY WORDS: Mitochondria, Soluble adenylyl cyclase, SAC, Calcium, IP3R, Oxidative phosphorylation

INTRODUCTION

Cyclic AMP (cAMP) has been implicated in a wide variety of (often contradictory) physiological processes, including different aspects of cell proliferation, apoptosis, differentiation, migration, development, ion transport, pH regulation and gene expression. A long-standing challenge in cAMP biology has been to understand how this single second messenger can simultaneously mediate so many disparate processes. This conundrum was especially puzzling when examining a single cell type. For example, Brunton and co-workers found that different hormones elicited distinct responses in a single cell type, yet both hormones worked via classic and defined cAMP signaling cascades (Buxton and Brunton, 1983, 1986). They postulated that cAMP signals in physically separated compartments within a cell. Functional compartmentalization of cAMP signaling was ultimately demonstrated for membrane-anchored and membrane-proximal, hormone-initiated signaling cascades (Davare et al., 2001; Marx et al., 2002), and it is now widely accepted that cAMP acts locally within independently regulated, spatially restricted compartments comprised of anchoring proteins (e.g. AKAPs) as well as the enzymes which synthesize (i.e. adenylyl cyclases; ACs) and degrade (i.e. phosphodiesterases; PDEs) cAMP.

A number of distinct cAMP compartments affect mitochondria (Monterisi and Zaccolo, 2017). Inside the matrix, cAMP is synthesized by the HCO_3^- and Ca^{2+} sensitive soluble adenylyl cyclase (sAC) in response to both metabolically generated CO_2/HCO_3^- (Acin-Perez et al., 2009b), as well as to the entry of Ca^{2+} through the mitochondrial Ca^{2+} uniporter (MCU) upon its release from the endoplasmic reticulum (ER) (Di Benedetto et al., 2014, 2013; Lefkimmiatis et al., 2013). sAC activation in mitochondria regulates OXPHOS and ATP production, (Acin-Perez et al., 2009b; Di Benedetto et al., 2013), and this pathway appears to be conserved in yeast (Hess et al., 2014).

Important additional roles of cAMP in mitochondria depend on signaling occurring outside the matrix, at the outer mitochondrial membrane, where a cAMP/PKA/PDE2A2 signaling domain regulates mitochondrial dynamics through phosphorylation of the fission protein Drp1 (Monterisi et al., 2017). Monterisi and co-workers also demonstrated that cAMP signaling of the outer mitochondrial membrane depends on PDE sculpting of second messengers generated at the plasma membrane by hormone and G-protein-regulated transmembrane adenylyl cyclases (tmACs).

Here, we find that the intramitochondrial sAC-defined domain regulates biogenesis of the OXPHOS complex by initiating a signaling cascade to the nucleus and uncover a novel extramitochondrial sAC-defined domain that regulates inositol 3-phosphate receptor (IP3R) phosphorylation, metabotropic Ca^{2+} release from the ER, and the functional coupling between ER Ca^{2+} and mitochondrial OXPHOS.

RESULTS

OXPHOS is impaired in sAC knockout MEFs

We investigated mitochondrial bioenergetic properties in mitochondria isolated from sAC knockout (KO) mouse embryonic fibroblast (MEF) cell lines in which the enzyme had been genetically ablated, and mitochondria isolated from isogenic wild type (wt) control MEFs (Bitterman et al., 2013; Rahman et al., 2016; Ramos-Espiritu et al., 2016a,b). Complex I (CI) physiological activity [NADH:decylubiquinone (DBQ) oxidoreductase activity], was significantly decreased in sAC KO cells. (Fig. 1A). Furthermore, the NADH oxidoreductase activity of CI measured by using an artificial electron acceptor (NADH:hexaammineruthenium oxidoreductase activity, HAR), which indicates the total amount of flavin-containing CI, was similar in sAC KO and wt mitochondria (Fig. 1B). As a result, the DBQ:HAR ratio was significantly

[1]Brain and Mind Research Institute, New York, NY 10065, USA. [2]Department of Pharmacology, Weill Cornell Medicine, New York, NY 10065, USA. [3]High-Throughput and Spectroscopy Resource Center, The Rockefeller University, New York, NY 10065, USA.

*Author for correspondence (gim2004@med.cornell.edu)

G.M., 0000-0003-0682-0731

Received 15 May 2017; Accepted 29 August 2017

Journal of Cell Science (2017) 130, 3713-3727 doi:10.1242/jcs.206318

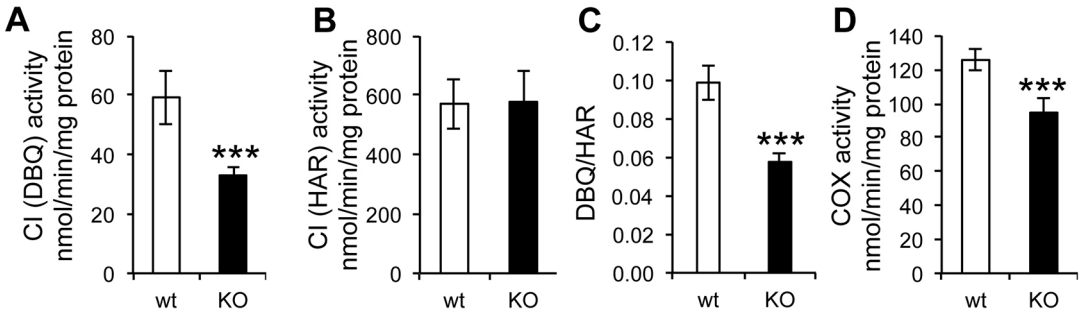

Fig. 1. Complex I and Complex IV activities are decreased in sAC KO MEFs. (A) NADH:DBQ oxidoreductase activity (DBQ) (Complex I activity) (n=8). (B) NADH:HAR oxidoreductase activity (HAR) (n=8). (C) DBQ:HAR ratio (n=8). (D) COX activity (n=8). Data are expressed as mean±s.e.m. in eight different biological replicates (***P<0.001, Student's t-test).

decreased in sAC KO MEFs (Fig. 1C), indicating a decrease in activity but not a loss of CI content (i.e. the number of enzyme molecules per mg of mitochondrial protein). In addition, sAC KO mitochondria displayed a small decrease in cytochrome *c* oxidase (complex IV, COX) activity compared to wt (Fig. 1D), supporting the notion that COX is regulated by sAC (Acin-Perez et al., 2009a).

To study intact cell energy metabolism, the mitochondrial oxygen consumption rate (OCR) and extracellular acidification rate (ECAR) were measured in a flux analyzer. In sAC KO MEFs, OCR was significantly decreased (Fig. 2A) while ECAR was increased (Fig. 2B), indicating lower cell respiration and greater lactate production. The OCR:ECAR ratio was decreased in sAC KO cells (Fig. 2C), suggesting a shift toward glycolytic metabolism. The maximal OCR achieved upon addition of the uncoupler carbonyl cyanide-p-trifluoromethoxyphenylhydrazone (FCCP) was similar in sAC KO and wt cells (Fig. 2D), indicating that sAC regulates respiration only in coupled (i.e. ADP-phosphorylating) mitochondria. Accordingly, mitochondrial ATP synthesis was significantly decreased in sAC KO cells (Fig. 2E). Since it had been shown that PKA phosphorylates and inactivates mitochondrial IF1, a negative modulator of the F_1F_0 ATPase (García-Bermúdez et al., 2015), we investigated whether the absence of SAC affected IF1 phosphorylation. However, we did not detect IF1 phosphorylation in wt or sAC KO cells (data not shown), suggesting that IF1 phosphorylation is marginal in MEFs.

To exclude that the OXPHOS impairment associated with sAC KO was specific to one MEF line, ATP synthesis and COX defects were also confirmed in an independent sAC KO MEF line (sAC KO2 MEF, Fig. S1A,B).

In addition, the mitochondrial membrane potential ($\Delta\Psi$m) assessed as the accumulation of the potentiometric fluorescent probe tetramethylrhodamine methyl ester (TMRM) was lower in sAC KO than in wt cells (Fig. 2F,G), while in both lines FCCP completely dissipated $\Delta\Psi$m, indicating equal loading of the probe (Fig. 2F).

We then measured the ability of cells to proliferate in regular glucose-containing medium or under obligatory oxidative conditions, induced by replacing glucose with galactose (Robinson, 1996). In glucose medium, sAC KO cells displayed better growth, both at 48 h and 72 h, but not at 24 h, compared to wt MEFs (Fig. 2H). In contrast, in galactose medium, the growth of sAC KO cells was significantly decreased in respect to wt (Fig. 2I), further demonstrating that sAC KO cells had defective mitochondrial energy production.

sAC KO increases the content of OXPHOS components

In light of the decrease in mitochondrial respiration and ATP synthesis in sAC KO MEFs, we investigated the steady-state levels of OXPHOS proteins. Surprisingly, western blots of cell homogenates revealed that sAC KO MEFs had increased levels of the mitochondrial NADH:ubiquinone oxidoreductase subunit B8 (NDUFB8) of CI, the 30-kDa subunit of CII, core 2 of complex III, subunit 1 of COX and the α-subunit of complex V, relative to levels of β-actin (Fig. 3A,B). However, the increase in the levels of mitochondrial proteins was selective and did not involve all proteins because the voltage-dependent anion channel protein (VDAC), the inner membrane translocator protein TIM23 and the matrix chaperone HSP60 were unchanged (Fig. 3A,B). Furthermore, in isolated mitochondria from sAC KO cells, subunit 1 of COX and subunit NDUFB8 of complex I were significantly increased relative to TIM23 but were not increased in other OXPHOS subunits (Fig. S2A,B).

The levels of PKA were also unchanged, suggesting that lack of sAC did not affect the expression of the cAMP effector. Since it had been shown that transfection efficiency of another cAMP effector, the exchange protein activated by cAMP 1 (EPAC1, officially known as RAPGEF3), modulates mitochondrial function in response to stimulation with Ca^{2+} or HCO_3^- (Wang et al., 2016), we investigated EPAC1 expression levels, which were unchanged in the absence of sAC (Fig. 3A,B). sAC KO cells also contained more mtDNA (COX1 gene) relative to nuclear DNA (18S rRNA gene) than wt (Fig. 3C). In addition, the average area occupied by mitochondria in each cell, visualized by microscopy with the non-potentiometric fluorescent dye MitoTracker Green FM, was increased in sAC KO MEFs (Fig. 3D). No significant differences were detected between wt and sAC KO MEFs regarding mitochondrial morphology, aspect ratio and form factor (Fig. S3A, B,C). The increase in OXPHOS proteins, mtDNA and mitochondrial density suggests that sAC KO cells had greater mitochondrial content than wt.

Taken together, these data suggest that sAC KO cells had increased mitochondrial content and a selective increase of OXPHOS proteins and mtDNA. However, other mitochondrial proteins did not increase proportionally, which might explain why sAC KO cells had impaired OXPHOS function, despite the increase in several OXPHOS components.

AMP-activated protein kinase (AMPK) is a key regulator of cellular energy homeostasis that is involved in mitochondrial biogenesis and is activated by phosphorylation (Hardie, 2007; Shaywitz and Greenberg, 1999). In sAC KO MEFs, the ratio between phopshorylated AMPK (P-AMPK) and AMPK (P-AMPK: AMPK) was increased (Fig. 3E,F), indicating that the AMPK signaling pathway was activated. Accordingly, the mRNA levels of two downstream effectors of AMPK involved in mitochondrial biogenesis, PGC-1α (also known as *PPARGC1A*) (Fig. 3G) and

Journal of Cell Science (2017) 130, 3713-3727 doi:10.1242/jcs.206318

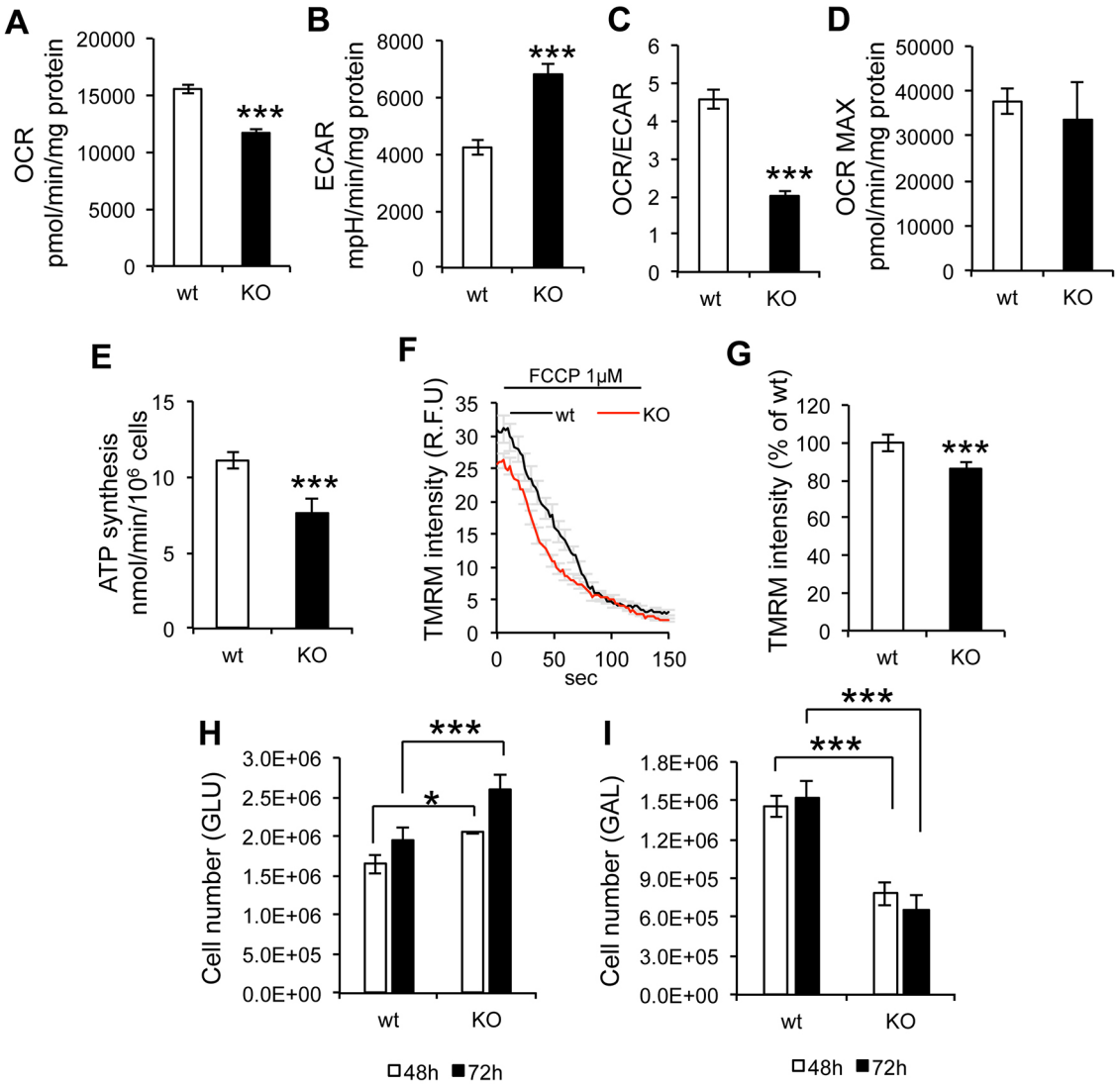

Fig. 2. Mitochondrial respiration, ATP synthesis and membrane potential are impaired in sAC KO MEFs. (A) Oxygen consumption rate (OCR, *n*=3). (B) Extracellular acidification rate (ECAR, *n*=3). (C) OCR/ECAR ratio (*n*=3). (D) Maximal OCR (*n*=3). (E) Mitochondrial ATP synthesis (*n*=6). (F) Trace of TMRM fluorescence in cells, before and after the addition of FCCP (1 µM). (G) TMRM average intensity of KO MEFs expressed as % of wt (*n*=3, >60 cells measured in each experiment). (H) wt and sAC KO MEFs were seeded at a density of 0.4×10^6 cells per well and cultured in glucose medium. Cells were counted at 48 and 72 h (*n*=3). (I) wt and sAC KO MEFs were seeded at a density of 0.4×10^6 cells per well, and cultured in galactose medium. Cells were counted at 48 and 72 h (*n*=3). Data are expressed as mean±s.e.m. in indicated number of different biological replicates (**P*<0.05, ****P*<0.001, Student's *t*-test).

NRF1 (Fig. 3H), were also upregulated. Furthermore, to confirm the involvement of AMPK in the signaling pathway leading to PGC-1α activation, we treated cells with the AMPK inhibitor Dorsomorphin (compound C, 10 µM) overnight. Dorsomorphin did not alter levels of PGC-1α in wt cells, whereas, in sAC KO cells treated with Dorsomorphin, activation of PGC-1α expression was essentially prevented (Fig. 3I), indicating that AMPK phosphorylation is, indeed, involved in the pathway.

Since PGC-1α can also be activated by reactive oxygen species (ROS) (Han et al., 2010; Zmijewski et al., 2010), we tested the effects of a 72 h treatment with the antioxidant Trolox (500 µM), which was shown to decrease ROS in OXPHOS deficient cells (Distelmaier et al., 2012). Trolox did not abolish the difference in PGC-1α between sAC KO and wt MEFs (Fig. S3D), suggesting that ROS did not play a major role in regulating mitochondrial biogenesis in sAC KO cells. Taken together, the data suggest that loss of sAC induced an AMPK-driven adaptive mitochondrial biogenesis response to OXPHOS deficiency.

sAC exclusively targeted to mitochondria restores P-AMPK level and OXPHOS function in sAC KO MEFs

Because sAC can be found in multiple locations inside cells (Acin-Perez et al., 2009b; Zippin et al., 2003), we sought to determine if the bioenergetics and signaling effects of sAC KO were specifically caused by the lack of sAC in mitochondria. To this end, we transfected cells with an enzymatically active recombinant sAC that is exclusively targeted to mitochondria (mtsAC) (Acin-Perez et al., 2009a). mtsAC localization by immunofluorescence coincided with that of the mitochondrial protein TOM20, while an untargeted version of the construct (sAC) showed diffuse intracellular distribution (Fig. 4A). The transfection efficiency was 70–80% for both constructs. Western blot analyses showed that, by using antibodies against the

Journal of Cell Science (2017) 130, 3713-3727 doi:10.1242/jcs.206318

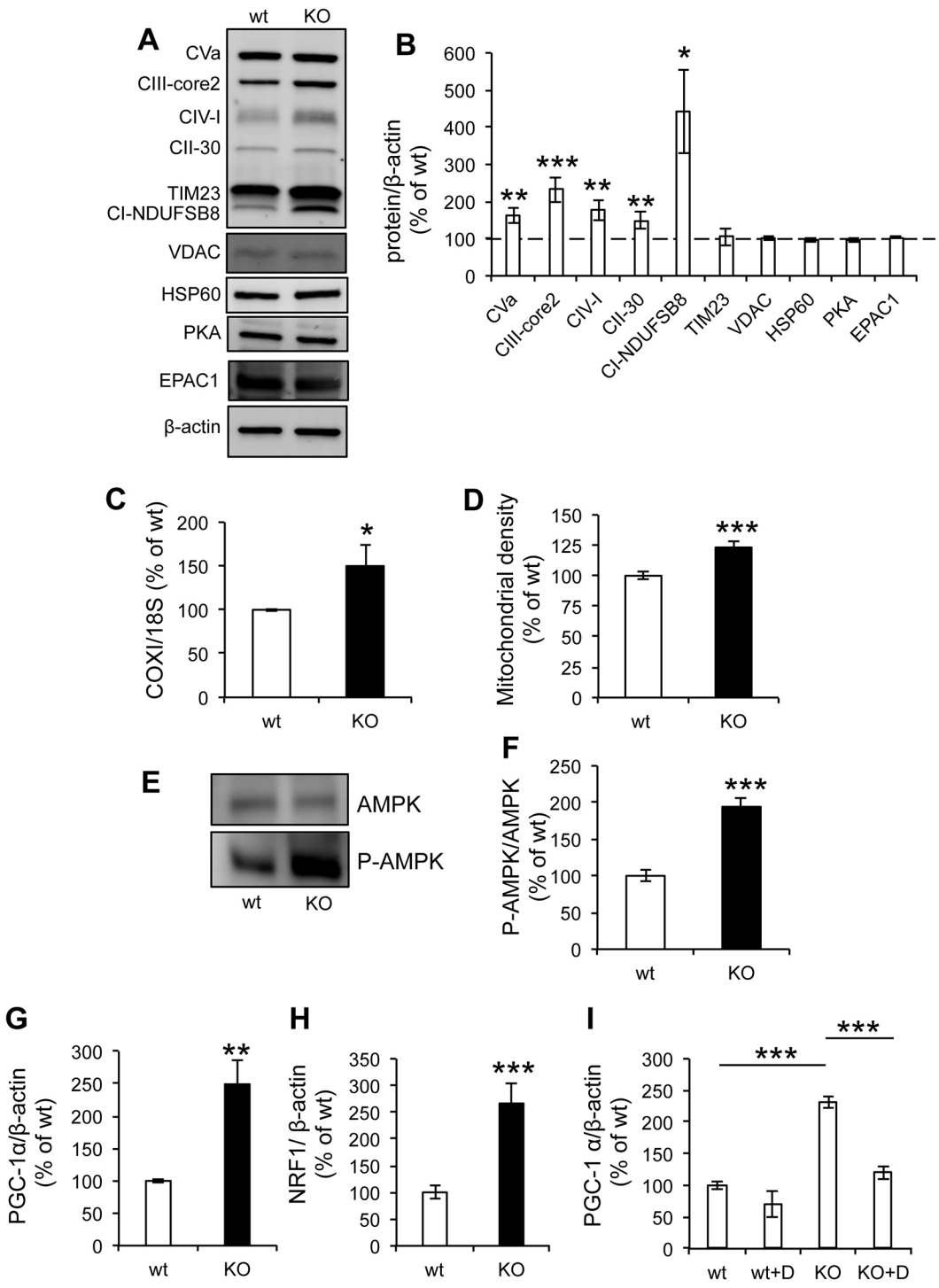

Fig. 3. OXPHOS protein complexes, mtDNA, mitochondrial content and mitochondrial biogenesis signaling are upregulated in sAC KO MEFs. (A) Western blot of OXPHOS complex subunits and structural components of the mitochondria machinery in cell homogenates (n=3–6). (B) Quantification of the relative contents of OXPHOS complexes normalized to β-actin (n=3–6). (C) mtDNA content measured by qPCR of the COX1 gene normalized to that of the 18S rRNA gene (n=4). (D) Mitochondrial density expressed as the average area of mitotracker-Green-labeled mitochondria in each cell (n=3, >20 cells per experiment). (E) Western blot of AMPK and P-AMPK (Tyr 172). (F) Quantification of the P-AMPK:AMPK intensity ratio (n=4). (G) PGC-1α mRNA levels relative to β-actin (n=4). (H) NRF1 mRNA levels relative to β-actin (n=4). All data are expressed as % of wt. Data are expressed as mean±s.e.m. in indicated number of different biological replicates (*P<0.05, **P<0.01, ***P<0.001, Student's t-test). (I) PGC-1α mRNA levels relative to β-actin in cells treated with (+D) or without Dorsomorphin (n=3). Data are expressed as mean±s.e.m. in indicated number of different biological replicates (***P<0.001, ANOVA with Tukey's correction).

hemagglutinin (HA) tag, KO MEFs transfected with sAC contained the protein in the enriched mitochondrial fraction, although at lower levels than cells transfected with mtsAC (Fig. 4B). In the cytosolic fractions, HA immunoreactivity was detected in the KO+sAC samples, whereas KO+mtsAC did not display any detectable signal.

At 48 h post transfection, sAC KO MEFs expressing sAC or mtsAC had significantly increased CI (DBQ/HAR) and

Journal of Cell Science (2017) 130, 3713-3727 doi:10.1242/jcs.206318

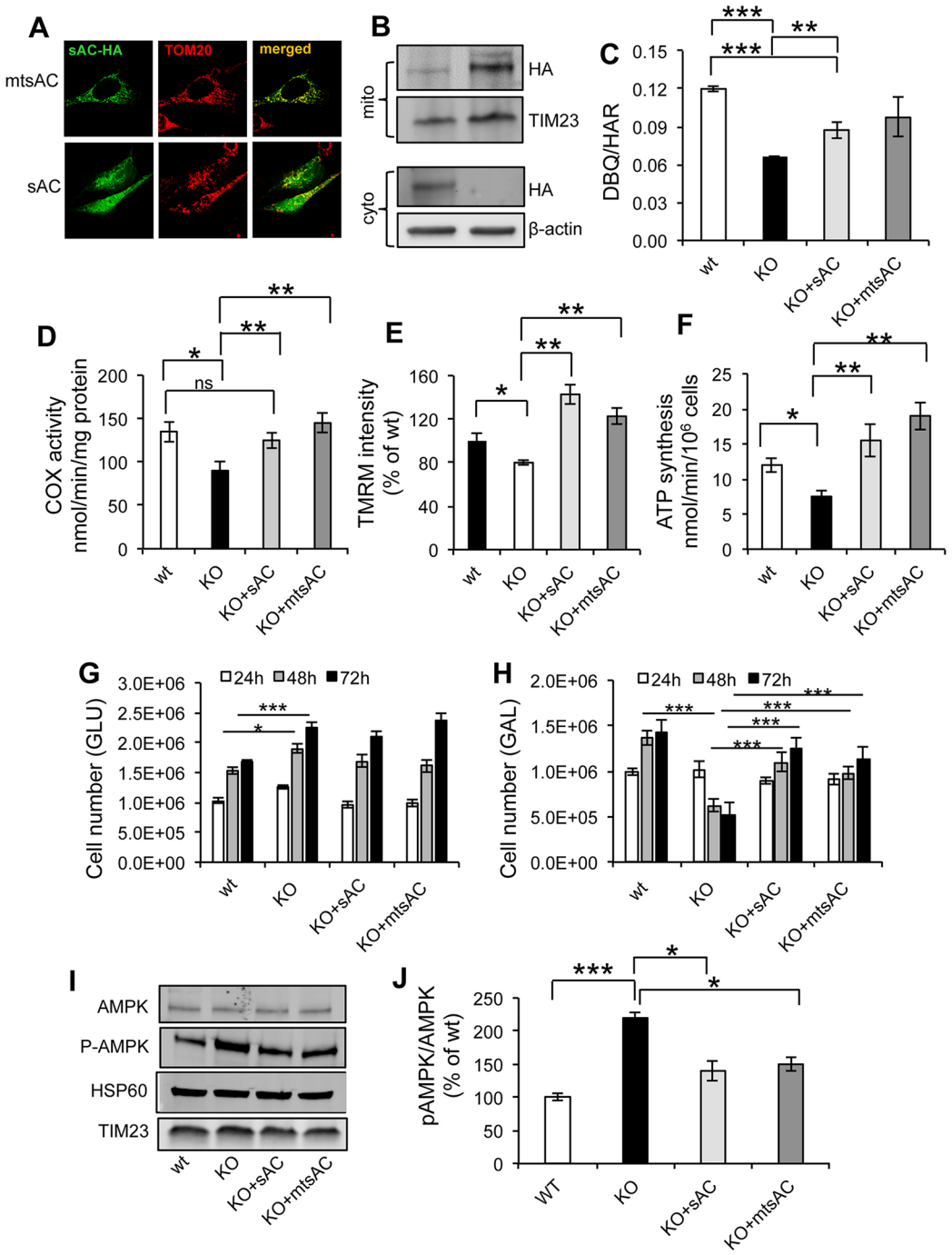

Fig. 4. Expression of mtsAC and sAC restores mitochondrial bioenergetics in sAC KO cells. (A) Representative images of sAC KO MEFs transfected with HA-tagged mtsAC-HA or HA-tagged sAC-HA and immunostained for HA (green) and TOM20 (red) antibodies. (B) Western blot of total cell homogenate and enriched mitochondrial fractions from KO MEFs transfected with sAC and mtsAC, and immunoblotted for HA, TIM23 and β-actin. (C) DBQ-HAR ratio of complex I activity in wt, KO, KO+sAC and KO+mtsAC (n=3). (D) COX activity in wt, KO, KO+sAC and KO+mtsAC (n=4). (E) TMRM average intensity (expressed as % of KO) in wt, KO, KO+sAC and KO+mtsAC (n=3). (F) ATP synthesis in wt, KO, KO+sAC and KO+mtsAC (n=4). (G) Cell number of wt, KO, KO+sAC and KO+mtsAC MEFs cultured for 24, 48 and 72 h in medium containing glucose. (H) Cell number of wt, KO, KO+sAC and KO+mtsAC cultured in medium containing galactose at 24, 48 and 72 h (n=3). The lines for statistical comparisons encompass both bars representing average values at 48 h and 72 h. (I) Western blot of AMPK, P-AMPK, HSP60, TIM23 in wt, KO, KO+sAC, KO+mtsAC and (J) P-AMPK:AMPK ratio expressed as % of wt (n=4). Data are expressed as mean±s.e.m. in indicated number of different biological replicates (*P<0.05, **P<0.01, ***P<0.001, ANOVA with Tukey's correction).

COX activities (Fig. 4C,D), as compared to sAC KO cells transfected with empty vector; and these activities were no longer significantly lower than in wt cells. TMRM accumulation (Fig. 4E) and mitochondrial ATP synthesis (Fig. 4F) were also increased by sAC and mtsAC expressed in sAC KO cells to levels comparable to wt. Furthermore, we investigated the cell growth of wt and sAC KO MEFs cultured in glucose or galactose medium. In glucose-containing medium, KO MEFs showed increased cell growth relative to wt that was not altered by expression of sAC or mtsAC (Fig. 4G). Importantly, in galactose

Journal of Cell Science (2017) 130, 3713-3727 doi:10.1242/jcs.206318

medium, KO MEFs transfected with sAC or mtsAC showed cell growth comparable to that in wt MEFs (Fig. 4H), confirming that sAC expression restored mitochondrial energy production in sAC KO cells.

In agreement with the hypothesis that increased mitochondrial biogenesis was the result of the lack of sAC in mitochondria, both sAC and mtsAC expression decreased the P-AMPK:AMPK ratio in sAC KO MEFs to levels comparable to those in wt cells (Fig. 4I,J). As expected, the levels of other mitochondrial proteins – such as HSP60 and TIM23, whose levels were unchanged in sAC KO MEFs – appeared unaffected by sAC or mtsAC overexpression (Fig. 4I). To further investigate the effect of mtsAC on KO cells, we analyzed the expression of the OXPHOS protein complexes in KO cells and KO+mtsAC cells 48 h after transfection. OXPHOS protein expression was decreased in KO+mtsAC cells compared to KO cells (Fig. S4A,B), but not complex V. Similarly the PGC1α mRNA expression (Fig. S4C) and the mtDNA content (Fig. S4D) were decreased in KO+mtsAC cells in respect to KO, indicating that mtsAC overexpression partially restored mitochondrial biogenesis in KO cells.

These results demonstrate that sAC localized in mitochondria is capable of improving mitochondrial bioenergetics and can extinguish the adaptive P-AMPK signaling of mitochondrial biogenesis.

ER-mitochondria Ca^{2+} transfer is altered in sAC KO MEFs

Mitochondria are key players in intracellular Ca^{2+} homeostasis, as they are able to accumulate Ca^{2+} from the cytosol through the mitochondrial Ca^{2+} uniporter (MCU) in a ΔΨm-dependent manner (De Stefani et al., 2015; Kamer and Mootha, 2015). Ca^{2+} release from the ER through the inositol-3-phosphate receptor (IP3R) is an essential signaling process that participates in the regulation of mitochondrial bioenergetics (Denton, 2009) and intramitochondrial sAC activity (Di Benedetto et al., 2014, 2013). To study the effect of sAC KO on ER-mitochondrial Ca^{2+} signaling, we utilized the fluorescent Ca^{2+} sensor GCaMP6 (Chen et al., 2013) targeted to the mitochondrial matrix (mitoGCaMP6). Mitochondrial localization of mitoGCaMP6 was assessed by co-transfection with a fluorescent reporter localized to mitochondria (mitoDsRed) (Fig. 5A). Upon Ca^{2+} release from the ER triggered by stimulation of purinergic receptors with ATP (1 mM, for 30 s, in perfusion buffer containing 1 mM Ca^{2+}), mitoGCaMP6 fluorescence increased (Fig. 5B), indicating mitochondrial Ca^{2+} uptake. As expected, treatment with FCCP (1 µM) to depolarize mitochondria prior to ATP stimulation resulted in a complete disappearance of the mitochondrial Ca^{2+} signal (Fig. 5C), demonstrating that the sensor specifically detected mitochondrial Ca^{2+}. After ATP stimulation, a small subset of sAC KO cells showed a mitochondrial Ca^{2+} response (33.1±10.1%) compared to that of wt cells (79.9±4.7%) (Fig. 5D), while the average mitoGCaMP6 fluorescence peak (F/F0) in responding cells was similar in wt and sAC KO cells (Fig. 5E). These results suggest that the probability of mitochondria taking up Ca^{2+} released from the ER was decreased in sAC KO cells.

The contacts between ER and mitochondria can be involved in the regulation of Ca^{2+} entry in mitochondria (Area-Gomez et al., 2012; Hayashi et al., 2009; Szabadkai and Rizzuto, 2004). Therefore, we investigated ER-mitochondria colocalization by transfecting cells with mitoDsRed and the fluorescent ER reporter Sec61-GFP. We did not detect differences in the colocalization of the two reporters between sAC KO and wt cells (Fig. S5A,B).

To test mitochondrial Ca^{2+} uptake of ER Ca^{2+} released in an IP3R-independent manner, we blocked the Ca^{2+} ATPase pump of the sarcoplasmic and endoplasmic reticulum with thapsigargin (TG, 1 µM). As expected, 100% of wt and sAC KO cells showed mitochondrial Ca^{2+} uptake upon TG addition (Fig. 5F). This result suggests that IP3R-dependent Ca^{2+} release was impaired in sAC KO cells, while ER Ca^{2+} content was unaffected. Interestingly, we also found that, upon TG stimulation, sAC KO cells had higher mitochondrial Ca^{2+} uptake than wt (Fig. 5G). Therefore, we investigated the levels of components that play a crucial role in the mitochondrial Ca^{2+} uptake machinery, such as MCU, its regulator mitochondrial calcium uptake protein 1 (MICU1) and the Na^{+}/Ca^{2+} exchanger SLC8B1 (hereafter referred to as NCLX). Normalized to TIM23, MCU (Fig. 5H,I) and NCLX (Fig. 5J,K) were significantly increased in sAC KO MEFs, whereas MICU1 was unchanged (Fig. 5L,M). We then measured Ca^{2+} uptake capacity in isolated mitochondria from wt and sAC KO MEFs by using Calcium Green-5N fluorescence, and found that sAC KO mitochondria had a higher capacity to take up Ca^{2+} from the buffer than wt (Fig. S5C).

Higher Ca^{2+} uptake in sAC KO MEFs can potentially be explained by a lack of cAMP-dependent activation of EPAC and consequent decreased inhibition of MCU by EPAC1 (Wang et al., 2016). Therefore, we tested mitochondrial Ca^{2+} uptake in wt and sAC KO cells treated with the EPAC1/2 inhibitor (ESI-09 10 µM) 30 min before treatment and throughout the measurements. Ca^{2+} release from the ER was induced with TG, ESI-09 did not significantly alter the amount of Ca^{2+} taken up by mitochondria, and the differences between wt and sAC KO persisted (Fig. S6A,B), suggesting that EPAC1 does not have significant impact on mitochondrial Ca^{2+} uptake in MEFs.

Taken together, these results indicate that sAC KO cells had decreased sensitivity to metabotropic stimulation of Ca^{2+} release from the ER. However, when ER Ca^{2+} was released in an IP3-independent manner using TG, mitochondria of sAC KO cells took up Ca^{2+} more efficiently, probably due to increased levels of MCU, accompanied by higher capacity of Ca^{2+} uptake, possibly resulting from increased levels of NCLX that prevented Ca^{2+} overload.

ER-mitochondrial Ca^{2+}-mediated functional coupling is altered in sAC KO MEFs

Since mitochondrial Ca^{2+} uptake has well-known regulatory functions on mitochondrial respiration (Denton, 2009), we measured OCR upon ATP stimulation of Ca^{2+} release from the ER. For these experiments, cells were treated with the uncoupler 3,5-di(tert-butyl)-4-hydroxybenzylidenemalononitril (SF6847), which allows for maximal electron transfer activity in the respiratory chain. ATP induced a small but significant increase in OCR in wt cells. In contrast, ATP did not affect sAC KO cells (Fig. 6A), consistent with their decreased probability of Ca^{2+} release from the ER. Furthermore, we monitored TMRM fluorescence of Ca^{2+} release from the ER upon stimulation with ATP and found that a smaller proportion of sAC KO cells (21.1±3%) showed an increase in TMRM fluorescence compared to wt cells (70±4%) (Fig. 6B). Last, we observed that the average intensity of the TMRM fluorescence peak in responding cells was lower in sAC KO cells compared to wt cells (Fig. 6C). This suggests that, even in the minority of responding cells that took up Ca^{2+} in mitochondria, the underlying bioenergetic defect attenuated the ΔΨm increase. Taken together, these results indicate that the absence of sAC decreases the probability of IP3R opening and as well as the defective coupling between metabotropic Ca^{2+} release from the ER and mitochondrial bioenergetics.

Journal of Cell Science (2017) 130, 3713-3727 doi:10.1242/jcs.206318

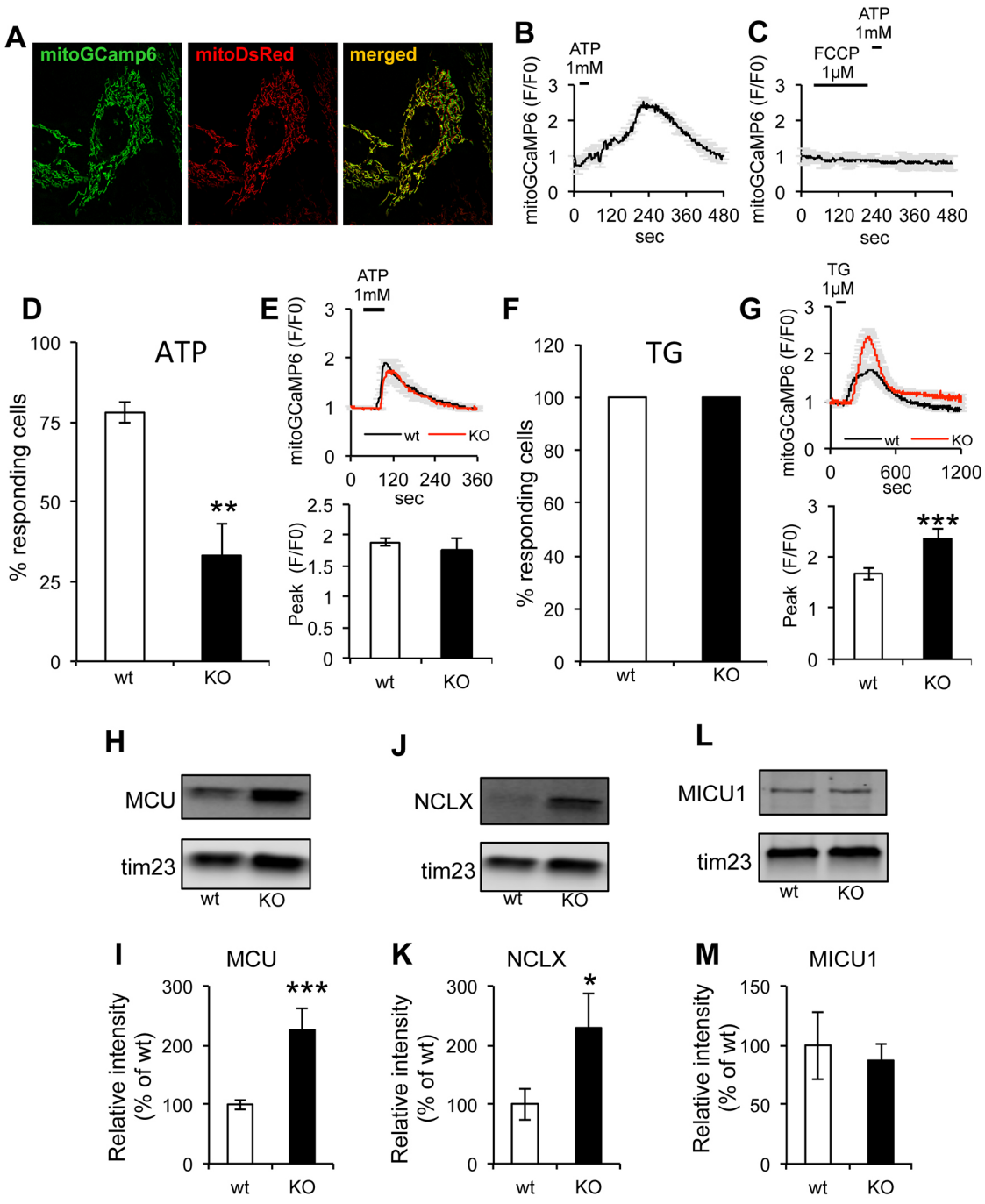

Fig. 5. Mitochondrial Ca^{2+} responses following stimulation of Ca^{2+} release from the ER is abnormal in sAC KO MEFs. (A) Representative image of wt MEFs co-transfected with mitoGCamp6 and mitoDsRed and merged images. (B) Representative average intensity curve of mitoGCamp6 upon ATP stimulation in wt cells (*n*=6 cells). (C) Average intensity of mitoGCamp6 in wt cells upon FCCP (first) and ATP (after) addition (*n*=3 cells). (D) Average percentage of responding wt versus KO cells upon ATP stimulation. (E) Top panel: curves of average mitoGCaMP6 fluorescence in MEFs stimulated with 1 mM ATP (*n*=14–78 cells, in three independent experiments). Bottom panel: quantification of mitoGCaMP6 fluorescence peak values in responding cells. (F) Percentage of responding cells upon stimulation with TG. (G) Top panel: average curve of mitoGCaMP6 fluorescence in wt and sAC KO MEFs stimulated with 1 μM TG (*n*=26–37 cells, in three independent experiments). Bottom panel: quantification of mitoGCaMP6 fluorescence peak values in responding wt and sAC KO cells. (H) Western blot of MCU in isolated mitochondria from wt and sAC KO MEFs (*n*=3) and (I) quantification of the relative intensity normalized on TIM23 and expressed as % of wt. (J,K) Western blot of NCLX in isolated mitochondria from wt and sAC KO MEFs (J) and quantification of the relative intensity normalized on TIM23 and expressed as % of wt (K). (L,M) Western blot of MICU1 in isolated mitochondria of wt and sAC KO cells (*n*=3) (L), and quantification of the relative intensity normalized on TIM23 and expressed as % of wt (M). Data are expressed as mean±s.e.m. in indicated number of different biological replicates (*P<0.05, **P<0.01, ***P<0.001, Student's *t*-test).

Metabotropic ER Ca^{2+} release is altered in sAC KO MEFs

We investigated if the decrease in the number of sAC KO cells that took up Ca^{2+} in mitochondria upon ATP stimulation is associated with alterations of Ca^{2+} release from the ER in the cytosol. By using the cytosolic Ca^{2+} reporter GCaMP6, we observed that ATP stimulation induced a cytosolic Ca^{2+} increase in the majority of wt

Journal of Cell Science (2017) 130, 3713-3727 doi:10.1242/jcs.206318

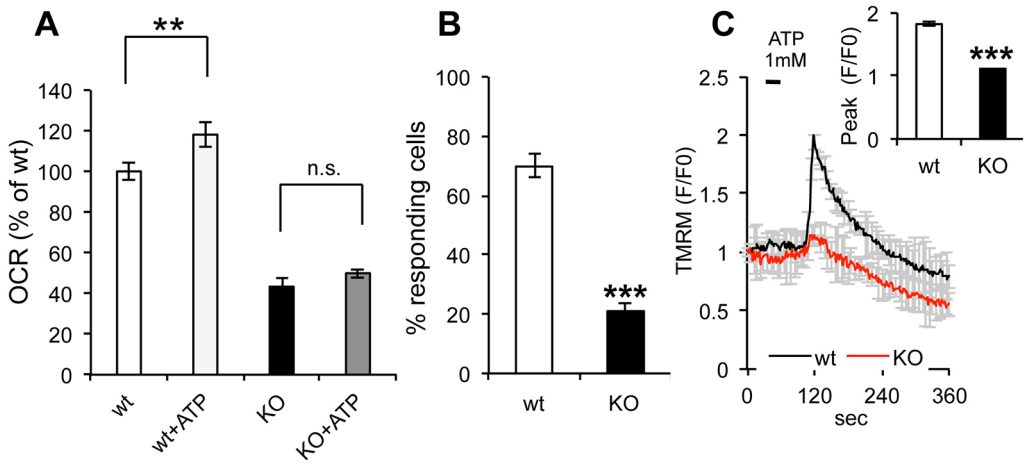

Fig. 6. ER-mitochondria bioenergetics is coupled through Ca^{2+} signaling. (A) OCR measured in uncoupled mitochondria (SF 1 µM) of wt and sAC KO cells in the presence or absence of ATP (*n*=3). (B) Percentage of responding wt and sAC KO cells loaded with fluo4 and stimulated with ATP 1 mM. (C) TMRM average intensity of wt and sAC KO MEFs upon ATP 1 mM stimulation and loaded with fluo4. Insert: peak average intensity of fluo4 in wt and sAC KO MEFs upon ATP stimulation (*n*=30–55, in 3 independent experiments). Data is expressed as mean±s.e.m. in indicated number of different biological replicates (***P*<0.01, ****P*<0.001, Student's *t*-test).

cells (80.3±3%), while the proportion of responsive sAC KO cells was significantly lower (42.4±8%) (Fig. 7A). Furthermore, the cytosolic Ca^{2+} peak height (F/F0) in the smaller subset of responsive sAC KO cells was lower than wt cells (Fig. 7B). Similarly to ATP, bradykinin (1 µM) stimulated fewer sAC KO cells, which also had lower cytosolic Ca^{2+} peaks (Fig. S7A,B), suggesting that ER Ca^{2+} signaling abnormalities were not due to changes in purinergic receptors or IP3 generation. Furthermore, upon TG (1 µM) administration, 100% of wt and sAC KO MEFs showed Ca^{2+} release from the ER (Fig. 7C) and the fluo4 fluorescence peaks were similar in the two cell lines (Fig. 7D), indicating that the decreased metabotropic ER Ca^{2+} response in sAC KO cells was not due to lower ER Ca^{2+} content.

Although the ryanodine receptor (RyR) has not been reported in fibroblasts we wanted to ensure that RyRs do not contribute to Ca^{2+} release from the ER in our system (Reiken et al., 2003). We, therefore, treated cells with the RyR inhibitor Dantrolene (10 µM for 1 h) prior to ATP administration. Dantrolene did not affect the proportion of cells that responded to ATP nor the difference in Ca^{2+} peak amplitude between sAC KO and wt cells (Fig. S7C,D), confirming that the RyR did not play a role in the metabotropic Ca^{2+} response in these cells.

Together, these results point to abnormal IP3R-mediated Ca^{2+} release from the ER in sAC KO cells.

Mechanisms of IP3R dysregulation in sAC KO MEFs

IP3R phosphorylation is involved in Ca^{2+} signaling (Vanderheyden et al., 2009). PKA phosphorylates mouse IP3R1, which is abundantly expressed in MEFs (Oakes et al., 2005), at two sites (S1588 and S1756; Ferris et al., 1991), leading to an increase in the probability of the Ca^{2+} channel being open (Nakade et al., 1994; Tang et al., 2003; Wagner et al., 2004). Therefore, we hypothesized that sAC KO impairs IP3R regulation by PKA-mediated phosphorylation.

We determined by western blot using phospho-IP3R1 antibodies that the levels of IP3R1 phosphorylated at S1756 (phospho-S1756) relative to total IP3R were decreased in sAC KO cells (Fig. 7E,F). Treatment of wt and sAC KO MEFs with calf intestinal alkaline phosphatase (CIP) caused a significant decrease of phospho-S1756 IP3R1 signal in both cell lines, confirming the specificity of the antibody (Fig. 7E). Furthermore, expression of recombinant sAC increased the levels of IP3R1 phospho-S1756 in sAC KO cells (Fig. S8A,B).

Pharmacological blockage of sAC in wt cells with the specific inhibitor KH7 (100 nM, for 30 min) resulted in a decrease in the proportion of cells that responded to ATP stimulation, similar to sAC KO cells (Fig. 7G). In addition, we assessed the effects of PKA inhibition on the probability of Ca^{2+} being released from the ER by using the PKA inhibitor H89 (1 µM), which resulted in a decrease of responding wt cells but not of sAC KO cells (Fig. 7H). The transmembrane adenylyl cyclase (tmAC) activator forskolin causes supraphysiological levels of cAMP t are able to simultaneously stimulate any cytoplasmic cAMP microdomain. Forskolin increased the probability of response in both wt and sAC KO MEFs, suggesting that tmAC-generated cAMP under pathophysiological conditions, is capable of reactivating the IP3R in sAC KO cells. Accordingly, IP3R phosphorylation was increased by forskolin in sAC KO cells, whereas KH7 decreased IP3R phosphorylation in wt but not in sAC KO cells (Fig. S8C,D).

Taken together, these data highlight a novel role for sAC in modulating IP3R activity, and indicate that defective PKA-dependent IP3R phosphorylation result in decreased probability of IP3R opening in sAC KO cells.

IP3R regulation is mediated by an sAC-defined cAMP functional domain and is not due to the mitochondrial effect

To discriminate whether defective ER Ca^{2+} signaling is due to lack of mitochondrial or cytosolic sAC we expressed HA-tagged mtsAC or HA-tagged sAC in sAC KO MEFs. Cells were co-transfected with mitoDsRed, which demonstrated that HA expression co-existed with mitoDsRed in ~90% of the transfected MEFs (Fig. S8E). mtsAC did not increase the number of mitoDsRed-positive sAC KO cells in which Ca^{2+} was released from the ER into the cytosol in response to ATP (wt=71.2±7.1%, sAC KO=24.5±3%, sAC KO+mtsAC=15.3±2.9%,) (Fig. 8A). The height of the cytosolic Ca^{2+} peak (F/F0) was also unchanged by the expression of mtsAC (Fig. 8B). By contrast, sAC expression increased the proportion of responding sAC KO cells (57.3±3.6%) (Fig. 8A), although the Ca^{2+} peak was only modestly increased (by 16.4%, Fig. 8B), suggesting that sAC expression partially rescued

Journal of Cell Science (2017) 130, 3713-3727 doi:10.1242/jcs.206318

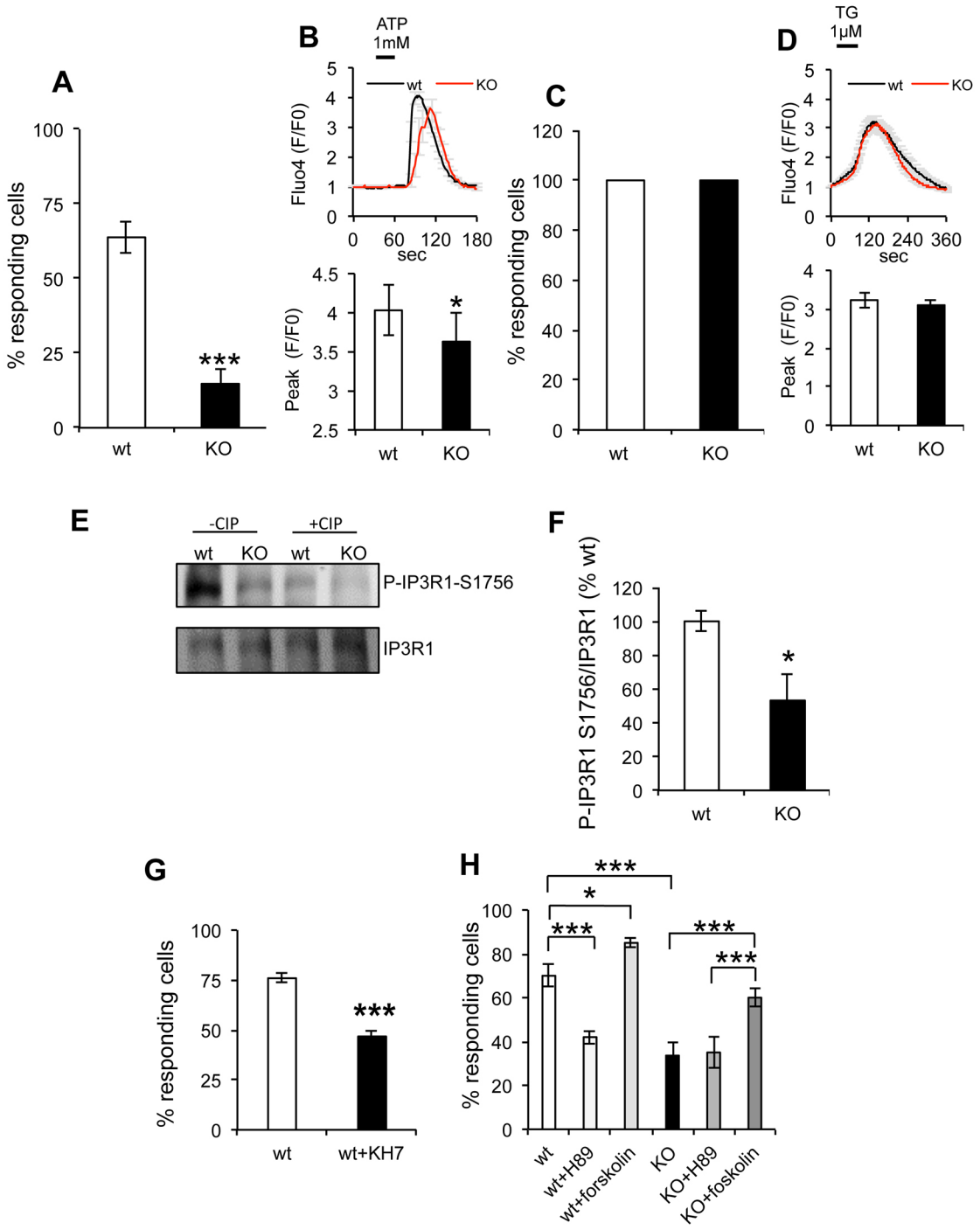

Fig. 7. Cytosolic Ca^{2+} release by the ER and uptake by the mitochondria is impaired in sAC KO MEFs and IP3R phosphorylation is decreased in sAC KO MEFs. (A) Percentage of wt and sAC KO cells responding to ATP stimulation. (B) Top panel: average Fluo4 fluorescence in wt and sAC KO MEFs stimulated with 1 mM ATP (n=18–32 cells, in three independent experiments). Bottom panel: quantification of Fluo4 fluorescence peak values in responding wt and sAC KO cells. The majority of the KO cells do not show variation in the Ca^{2+} concentration upon ATP stimulation, in contrast to wt cells. (C) Percentage of cells responding to TG stimulation of ER Ca^{2+} release; there is no difference between wt and KO cells. (D) Top panel: curves of average fluo4 fluorescence in MEFs stimulated with 1 μM TG (n=165–254 cells, in three independent experiments). Bottom panel: quantification of fluo4 fluorescence peak values in responding wt and sAC KO cells. (E) Western blot of IP3R1 P-Ser1756 and IP3R1 in wt and sAC KO cells in the absence or presence of CIP. (F) Quantification of the P-IP3R1 Ser1756:IP3R1 ratio expressed as a % of wt (n=6). (G) Percentage of responding wt and sAC KO cells loaded with fluo4 and pretreated with KH7 100 mM for 30 min. Data are expressed as mean±s.e.m. in indicated number of different biological replicates (*P<0.05, ***P<0.001, Student's t-test). (H) Percentage of responding wt and sAC KO cells loaded with Fluo4 upon ATP stimulation and treated with the sAC inhibitor H89 1 μM or the tmAC activator forskolin 50 μM (n=3). Data are expressed as mean±s.e.m. in indicated number of different biological replicates (*P<0.05, ***P<0.001, ANOVA with Tukey's correction).

metabotropic ER Ca^{2+} signaling. These results indicate that impaired sensitivity to metabotropic stimulation was due to lack of sAC-mediated modulation of IP3R and not to mitochondrial effects of sAC KO. As expected, mitochondrial Ca^{2+} uptake measured with mitoGCaMP6 in sAC KO cells after ATP stimulation was not restored by mtsAC (Fig. 8C,D). Also, sAC expression failed

Journal of Cell Science (2017) 130, 3713-3727 doi:10.1242/jcs.206318

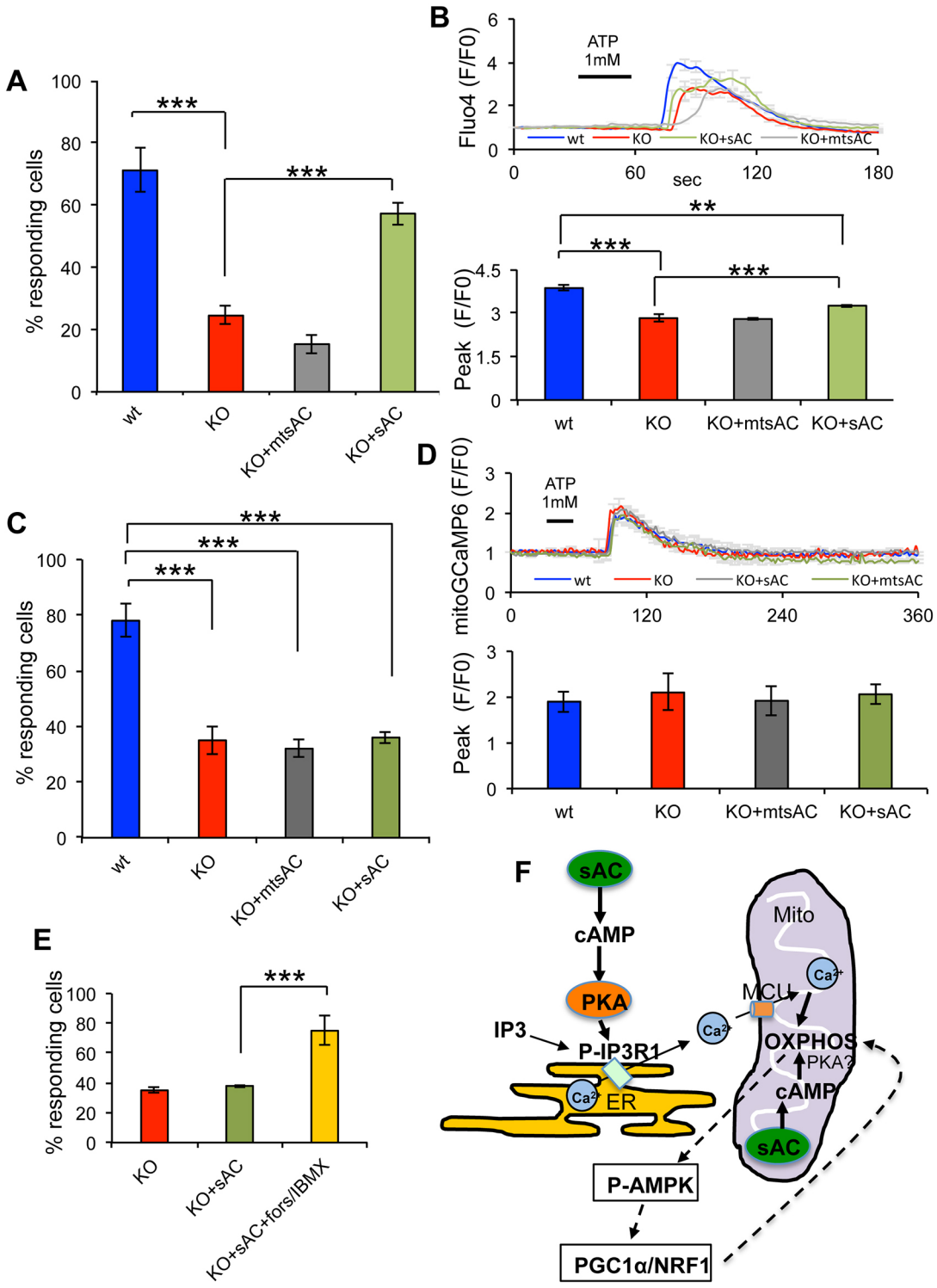

Fig. 8. sAC and mtsAC expression restores ER Ca^{2+} release in sAC KO MEFs. (A) Percentage of cells responding to ATP stimulation in wt, KO, KO+mtsAC and KO+sAC MEFs and loaded with fluo4. (B) Top panel: average fluo4 fluorescence in MEFs stimulated with 1 mM ATP. Bottom panel: quantification of the peak values in responding cells (n=29–52 cells, in three independent experiments). (C) Percentage of cells responding to ATP stimulation in wt, KO, KO+mtsAC and KO+sAC MEFs and loaded with mitoGCaMP6. (D) Top panel: average mitoGCaMP6 fluorescence in MEFs stimulated with 1 mM ATP. Bottom panel: quantification of the peak values in responding cells (n=35–42 cells, in three independent experiments). Data are expressed as mean±s.e.m. in indicated number of different biological replicates (***P<0.001, ANOVA with Tukey's correction). (E) Percentage of cells responding to ATP stimulation in KO, KO+sAC and KO+sAC treated with forskolin/IBMX and loaded with mitoGCaMP6 (n=30–54 cells, in three independent experiments). Data are expressed as mean±s.e.m. in indicated number of different biological replicates (***P<0.001, Student's t-test). (F) Schematic representation of sAC-cAMP domains that regulate ER Ca^{2+} signaling and OXPHOS: cytosolic sAC produces cytosolic cAMP that leads to PKA-mediated phosphorylation and activation of the IP3R in the ER membrane and increased probability of the open state upon IP3 stimulation. Ca^{2+} from the ER is taken up by MCU and activates mitochondrial OXPHOS. Mitochondrial sAC regulates OXPHOS in a cAMP-mediated manner, independently of cytosolic sAC. The involvement of PKA as the cAMP-activated kinase in the mitochondrial matrix remains controversial (Valsecchi et al., 2014). OXPHOS regulates the PGC1α/NRF1 signaling pathway through P-AMPK.

Journal of Cell Science (2017) 130, 3713-3727 doi:10.1242/jcs.206318

to increase mitochondrial Ca^{2+} uptake in sAC KO cells (Fig. 8C,D), despite the modest increase observed in the cytosolic Ca^{2+} peak (Fig. 8B), presumably because the Ca^{2+} concentration in the cytosol did not reach a sufficient threshold to activate the MCU. In order to confirm this hypothesis, mitochondrial Ca^{2+} was measured in KO +sAC cells and in KO+sAC cells co-treated with forskolin and IBMX (forskolin/IBMX) and the number of cells responding to ATP stimulation was quantified. Addition of forskolin/IBMX in KO +sAC cells significantly increased the number of responding cells compared to KO+sAC (Fig. 8E), indicating that the Ca^{2+} concentration must reach a threshold to activate the MCU.

DISCUSSION

The intramitochondrial sAC-defined cAMP compartment regulates mitochondrial energy production. In sAC KO MEFs, where this regulation is chronically absent, cells respond with a compensatory increase of biogenesis of the OXPHOS complex. sAC KO MEFs also exhibit impaired coupling of ER Ca^{2+} and OXPHOS. In sAC KO MEFs, Ca^{2+} entry into mitochondria after stimulating Ca^{2+} release from the ER is diminished, and this attenuation is caused by desensitization of the IP3R to metabotropic stimulation. In contrast to mitochondrial bioenergetics and biogenesis of the OXPHOS complex, the cAMP-dependent regulation of IP3R Ca^{2+} release is controlled by extramitochondrial sAC. Our identification of an intramitochondrial domain that regulates OXPHOS, and an extramitochondrial domain that modulates the coupling between Ca^{2+} release from the ER and OXPHOS, defines multiple distinct sAC-regulated cAMP signaling compartments that affect mitochondrial function.

The original studies by Brunton et al., suggesting that second messenger signaling had to be compartmentalized, were performed in cardiac myocytes. Stimulation with β-adrenergic agonists increased contractility whereas prostaglandins altered metabolism; and both seem to be mediated via cAMP and PKA (Buxton and Brunton, 1983, 1986). In these studies, the molecular details of the distinct compartments had not been identified but, since both β-agonists and prostaglandins signal via GPCRs, functionally distinct plasma membrane-bound tmAC-dependent compartments were postulated. Ultimately, theories of compartmentalization were confirmed by studies demonstrating that hormones can stimulate functionally separate tmAC-dependent cAMP compartments (Davare et al., 2001; Marx et al., 2002), and current models of cAMP signaling are dependent upon compartmentalization of the second messenger into independently regulated cAMP-signaling domains (Lefkimmiatis and Zaccolo, 2014).

We have previously demonstrated that HCO_3^-- and Ca^{2+}-sensitive sAC is distributed throughout the cell (Zippin et al., 2003), which suggests that cAMP can be generated locally to fuel signaling at intracellular cAMP compartments (Bundey and Insel, 2004). One such sAC-defined intracellular compartment is the mitochondrial matrix, where cAMP generated by sAC regulates OXPHOS (Valsecchi et al., 2013). For other intracellular cAMP compartments, the situation has been less clear. A variety of studies suggest that sAC can generate cAMP locally; for example, on trafficking endosomes (Inda et al., 2016). However, other results point to PDE activity that regulates intracellular cAMP compartments and originates from second messengers produced by tmACs (Monterisi et al., 2017). Data presented here demonstrate that cAMP regulates Ca^{2+} release from the ER via an extramitochondrial, sAC-defined signaling domain. Thus, cells contain at least two distinct sAC-regulated cAMP compartments that control mitochondrial function, one inside the matrix and a second one outside, in addition to the outer membrane tmACs-mediated cAMP regulation of mitochondrial dynamics. There may be other sAC-defined cAMP compartments revealed by additional phenotypes in sAC KO MEFs. We have previously shown that sAC KO MEFs display a lysosomal acidification defect (Rahman et al., 2016) and are more susceptible to oncogenic transformation than wt cells (Ramos-Espiritu et al., 2016a). However, neither of these phenotypes has been ascribed to a specifically localized isoform of sAC, so it is unclear whether they define unique cAMP functional compartments.

The absence of sAC impairs mitochondrial energy metabolism by causing a decline in CI activity, COX activity, cell respiration, $\Delta\Psi m$, ATP production and impaired growth in galactose medium. Furthermore, sAC KO cells display a shift towards glycolytic metabolism, as indicated by a decreased OCR:ECAR ratio. Taken together, these results are consistent with data obtained by using pharmacological modulators of the enzyme (Acin-Perez et al., 2009a,b; De Rasmo et al., 2015; Di Benedetto et al., 2013). In addition, recent reports have shown that pharmacological inhibition of sAC causes CI activity defects in fibroblasts (De Rasmo et al., 2015), and silencing of sAC resulted in decreased TMRM accumulation potential in cardiomyocytes (Wang et al., 2016). Importantly, we demonstrate that bioenergetic defects in sAC KO cells are due to the loss of the matrix sAC-defined cAMP domain, since they can be fully rescued by expression of a recombinant sAC that is selectively targeted to the mitochondrial matrix. Importantly, we find that the effects of sAC ablation extend to broader intracellular signaling mechanisms involving biogenesis of the OXPHOS complex – possibly as an adaptive response to energy depletion – and which are also complemented by targeting sAC to the matrix.

Energy deprivation induces activation of AMPK, one of the key enzymes responsible for the regulation of mitochondrial biogenesis (Scarpulla, 2011). AMPK is activated by phosphorylation and maintains energy homeostasis by promoting catabolism and inhibiting ATP consuming processes (Hardie et al., 2012; Witczak et al., 2008). Since AMPK can be phosphorylated by PKA in a cAMP-dependent manner (Hawley et al., 2010), it can be expected that sAC KO MEFs have less P-AMPK. Instead, levels of P-AMPK are upregulated in sAC KO MEFs. Therefore, a cAMP-independent mechanism may be involved. For example, AMPK can be phosphorylated by liver kinase B1 (LKB1, officially known as STK11), a serine/threonine protein kinase activated under conditions of energy deprivation (Ruderman et al., 2010). Another mechanism of AMPK phosphorylation is through Ca^{2+}/calmodulin-dependent protein kinase kinase 2 (CaMKK2). However, since this kinase is activated by increased cytosolic Ca^{2+} levels and because Ca^{2+} release from the ER is decreased in sAC KO MEFs, it is unlikely that CaMKK2 represents a major effector of AMPK phosphorylation in these cells. Another way to phosphorylate AMPK is through ROS production (Han et al., 2010; Zmijewski et al., 2010). However, the downstream effector PGC-1α was unaffected by antioxidants in sAC KO MEFs, suggesting that a reduction in intracellular ATP levels, rather than ROS, is responsible for AMPK phosphorylation. The activation of AMPK suggests that an energy deprivation response takes place in sAC KO cells, leading to a signaling cascade that increases biogenesis of the OXPHOS complex (Scarpulla, 2012). In support of this hypothesis, we observed that expression of the downstream effectors of P-AMPK, PGC-1α and NRF1, is upregulated in sAC KO MEFs. Furthermore, normalization of mitochondrial energy production by mtsAC decreases the level of P-AMPK.

Journal of Cell Science (2017) 130, 3713-3727 doi:10.1242/jcs.206318

Mitochondrial Ca^{2+} is a modulator of cellular energy homeostasis (Denton, 2009) and release of Ca^{2+} from the ER was shown to affect not only mitochondrial biogenesis but also signaling via AMPK (Cárdenas et al., 2010) and mitochondrial substrate transporters (Satrustegui et al., 2007). Furthermore, it has been reported that Ca^{2+} regulates sAC activity in mitochondria (Di Benedetto et al., 2014, 2013), highlighting a pathway of metabolic regulation that involves Ca^{2+}, sAC and energy production. Mitochondria in sAC KO cells take up more Ca^{2+} when Ca^{2+} release from the ER is caused in response to TG or when isolated mitochondria are exposed directly to Ca^{2+}. We interpret this observation in light of the increased complement of proteins involved in Ca^{2+} handling within mitochondria, notably MCU. However, sAC KO cells have attenuated cytosolic and mitochondrial Ca^{2+} responses upon metabotropic stimulation of Ca^{2+} release from the ER. We determined that this is not due to a lower Ca^{2+} concentration in ER stores but to a decrease in the phosphorylation of IP3R. Phosphorylation of IP3R1 increases the activity of the receptor (Ferris et al., 1991; Nakade et al., 1994; Tang et al., 2003; Wagner et al., 2004), and we find that sAC plays a role in this regulation. Lack of sAC-generated cAMP results in a decrease of PKA-mediated phosphorylation of IP3R1 within the ER and desensitization of the receptor, thereby lessening the probability of its open-state conformation that allows Ca^{2+} flux.

In conclusion, our data support the model (summarized in Fig. 8F), whereby signaling pathways initiated by distinct sAC-defined intra- and extramitochondrial domains converge in the fine-tuning of the regulation of cellular bioenergetics through ER-mitochondria Ca^{2+} signaling and biogenesis of the OXPHOS complex.

MATERIALS AND METHODS

MEF cultures

Wt and sAC KO MEFs were cultured in Dulbecco's modified Eagle's medium (DMEM) supplemented with 25 mM glucose, 110 mg/l pyruvate, 1% penicillin-streptomycin, and 5% fetal bovine serum (FBS). Where indicated, MEFs were cultured in galactose medium, in which glucose was substituted with 5 mM galactose, plus 5% dialyzed FBS. Cells were grown in galactose or glucose medium for 48−72 h and then counted in a particle counter (Coulter Beckman). The genotype of the cells was assessed by PCR by using the following primers: *wt sAC gene* forward 5′-TCTGGCCACA-CACTAAGG-3′, reverse 5′-CTCCAGCTCCGATGAAGG-3′; *KO sAC gene* forward 5′-CTGGGCTGTCCTCAAGCTC-3′, reverse 5′-GCAGCG-CATCGCCTTCTATC-3′. Cells were regularly tested for mycoplasma by using the free for mycoplasma test (Thermo Fisher Scientific, M7006).

Mitochondria isolation

Cells were grown to 70% confluence in P150 flasks, washed twice with phosphate-buffered saline (PBS) and scraped off into 2 ml of cold isolation buffer (in mM: 225 mannitol, 20 HEPES pH 7.4, 75 sucrose) containing a protease inhibitor cocktail (Roche Diagnostics) and phosphatase inhibitors (in mM: 1 NaF,1 Na_3VO_4, 1 pyrophosphate, 2 Imidazole). Cells were collected by centrifugation at 2000 ***g*** for 5 min at 4°C. The resulting pellet was resuspended in cold isolation buffer containing 1 mg/ml fatty acid-free BSA and homogenized on ice by using a glass-glass homogenizer. The homogenate was cleared at 800 ***g*** for 5 min at 4°C. The supernatant was centrifuged at 10,000 ***g***, for 10 min at 4°C. The resulting pellet containing the mitochondrial fraction was washed twice in isolation buffer, resuspended in 50−80 µl of isolation buffer, snap-frozen in liquid nitrogen and stored at −80°C.

OXPHOS function measurements

ATP synthesis was measured in cells (1.5×10^6) permeabilized with digitonin 50 µg/ml using a kinetic luminescence assay as described (Vives-Bauza et al., 2007). Pyruvate (5 mM) and malate (2 mM) were used as substrates. COX activity was measured spectrophotometrically in isolated mitochondria (5–10 µg of protein), as described (Birch-Machin and Turnbull, 2001). NADH-dependent enzymatic activities of Complex I were assayed spectrophotometrically using a Lambda 35 spectrophotometer (Perkin Elmer) or a SpectraMax plate reader (Molecular Devices) and expressed as a decrease in absorption at 340 nm (ε340 nm=6.22 mM^{-1} cm^{-1}) with 150 µM NADH in SET pH 7.5 (0.25 M sucrose, 0.2 mM EDTA, 20 µg/ml alamethicin, 1 mM $MgCl_2$, 50 mMTris-HCl) buffer containing 5–30 µg protein/ml of isolated mitochondria. For the measurement of NADH:DBQ (decylubiquinone) oxidoreductase activity, the concentrations of additions were 15−30 µg protein/ml, 45 µM DBQ, 1 mg/ml BSA (fatty acid-free) and 1 mM cyanide. The activity was sensitive to rotenone (1 µM). For the measurement of the ratio of NADH to hexaammineruthenium(III)-chloride (HAR) (NADH:HAR) oxidoreductase activity, isolated mitochondria (5−10 µg of protein per ml) were assayed in the presence of 1 mM cyanide with 1 mM HAR. The activities were measured at 25°C and expressed in nmol NADH×min^{-1}×mg^{-1}. NADH:DBQ oxidoreductase activity was normalized to complex I content as estimated from NADH:HAR reductase activities (DBQ divided by HAR).

Quantification of mitochondrial membrane potential and morphology

MEFs were incubated with 10 nM tetramethyl rhodamine methyl ester (TMRM) for 25 min at 37°C in DMEM. Cells were washed twice and then imaged in HEPES-Tris (HT) imaging buffer (in mM: 132 NaCl, 4.2 KCl, 1 $MgCl_2$, 5.5 D-glucose, 10 HEPES pH 7.4, 1 $CaCl_2$, with Tris base) at 37°C. Images from ten random fields per coverslips were acquired by using a Leica TCS SP5 Confocal Microscope (Leica Microsystems) with an oil-immersion 63× [1.4 (NA)] lens. Mitochondrial morphology was measured using Image Pro software (Universal Imaging) in cells loaded with Mitotracker Green (50 nM) for 25 min at 37°C as previously described (Koopman et al., 2006, 2005). Briefly, cells were imaged by using life-cell confocal laser scanning. Next, the acquired images were sequentially processed using an algorithm that yields quantitative descriptors for mitochondrial length and degree of branching (aspect ratio, AR; form factor, F) and the number of mitochondria per cell. In essence, the image-processing algorithm converts a background-corrected image into a binary image displaying mitochondrial structures (white) on a black background. This conversion consists of a number of subsequent calculations involving: (i) background correction of the acquired raw image, (ii) linear contrast optimization, (iii) top-hat filtering, (iv) median filtering and (v) thresholding (partitioning an image into a foreground and background).

OCR and ECAR measurement

Extracellular acidification rate (ECAR) and oxygen consumption rate (OCR) were determined using a Seahorse XF 96 flux analyzer (Seahorse Bioscience). MEFs were plated at 30,000/well. The next day the medium was replaced with KHB XF Assay medium supplemented with 1 mM sodium pyruvate and 1 mg/ml D-glucose (Sigma G5400) and incubated at 37°C in a non-CO_2 incubator for 1 h prior to the measurement. For normalization, protein determination of each well was done using DC™ Protein Assay kit (Biorad). To assess OCR after induction of Ca^{2+} release from the ER in wt and sAC KO cells, cells were treated with the biogenesis of the OXPHOS complex uncoupler SF6847 (Sigma, T182) to prevent matrix NADH accumulation, and then stimulated with ATP (1 mM).

Western blot electrophoresis

Cell homogenates or isolated mitochondria fractions were analyzed by western blot, as described before (Valsecchi et al., 2012). The following antibodies were used for protein detection: AMPKα, P-AMPKα (Thr172) (Cell signaling, cat. nos 2532 and 2531, respectively; 1:1000); IP3R and P-IP3R Ser 1756 (Cell Signaling, cat. nos 8568 and 3760, respectively; 1:500); EPAC1 (Cell Signaling, cat. no. 4155; 1:500); MCU (Sigma, cat. no. 16480; 1:1000); MCU1 (Abcam, cat. no. 102830; 1:1000); OXPHOS rodent cocktail (Abcam, cat. no. 110413; 1:1000); SLC24A6 (Abcam, cat. no.

83551; 1:1000); VDAC (Abcam, cat. no. 34726; 1:1000); HSP60 (Enzo Life Sciences, cat. no. 828; 1:1000); PKA (Upstate, cat. no. 06-903; 1:1000); β-actin (Sigma, cat. no. A5316; 1:1000). Appropriate fluorescently labeled secondary antibodies (Licor) were used for detection in the Odyssey CLx imaging system (Licor). For quantification of band intensities, the Image Studio Software package (Licor) was used. For the quantification of phosphorylated proteins, such as P-AMPK and P-IP3R, relative to the total protein, replicates of the samples were run in parallel. The blot was then cut and the two halves probed with the antibodies against phosphorylated protein or the antibodies against the total proteins.

IF-1 immunoprecipitation

Immunoprecipitation of ATPase inhibitory factor 1 (IF-1, officially known as ATPIF1) was performed using a co-immunoprecipitation kit (Thermo Scientific Pierce). Briefly, IF-1 antibody or normal mouse IgGs (ThermoFisher) were covalently coupled to IP resins. Mitochondria (0.5 mg) were resuspended in co-IP lysis/wash buffer (0.025M Tris-HCl, 0.15M NaCl, 0.001M EDTA, 1% NP-40, 5% glycerol; pH 7.4) and incubated with the resins overnight. Proteins were eluted in elution buffer (contains primary amine, pH 2.8) and eluates neutralized with Tris-HCl pH 8.5. Western blotting was performed with anti-IF-1 antibody to assess the presence of the target protein in the co-IP eluates. Two different antibodies against phosphorylated Ser/Thr (BD Biosciences, cat. no. 612548; 1:1000 and Cell Signaling, cat. no. 9621; 1:1000) were used to assess the phosphorylation of immunoprecipitated IF-1.

mtDNA and qPCR

Total DNA was isolated from cell pellets using the Wizard genomic DNA Purification kit (Promega). The abundance of the mtDNA COX1 gene was assayed by quantitative reverse transcription (qRT)-PCR using SYBR Green (Roche) in a Light Cycler (Roche). The 18S rRNA gene was used as an internal control. For mRNA analyses total mRNA was isolated from cells by using the RNAqueous-4PCR kit (Life Technology). cDNA was generated using the ImProm-II Reverse Transcription System (Roche). The relative mRNA levels of PGC1α and *NRF1* were determined by qRT-PCR and normalized by β-actin mRNA. Primers and PCR conditions were as follows. Primers used were: COX1 gene, forward 5′-CATCCCTTGACATCGTG-3′, reverse 5′-CTGAGTAGC GTCGTGG-3′. 18S rRNA gene, forward 5′-CGGACAGGATTGACAGA-3′, reverse 5′-CCAGTCAGTGTAGCGC-3′. PGC1α cDNA, forward 5′-TGAAAAAGCTTGACTGGCGTC-3′, reverse 5′-CGCTAGCAAGTTTGCCTCAT-3′. *NRF1* cDNA, forward 5′-CTTCATGGAGGAGCACGGAG-3′, reverse 5′-ATGAGGCCGTTTCCGTTTCT-3′. β-actin cDNA, forward 5′-CTTTGCAGCTCCTTCGTTGC-3′, reverse 5′-CCTTCTGACCCATTCCCACC-3′. Forward and reverse primers (10 µM) were mixed with the master mix SYBR Green (Roche), 25 mM Mg^{2+}, and H_2O, in the presence of 2.5 ng of DNA, according to the manufacturer's protocol.

PCR conditions: initial denaturation: 95°C 10 min; denaturation: 95°C 15 s, anneal: 50°C 10 s, extend: 72°C 15 s, 30 cycles; final extension: 72°C 10 min.

The reactions were optimized using a linear concentration range of DNA standards. In each experiment, samples were analyzed in triplicate.

Transgenic sAC and mtsAC expression

mt-sAC and sAC expression constructs have been previously described (Acin-Perez et al., 2009a). For imaging experiments, wt and sAC KO MEFs were transfected with sAC, mtsAC or empty vector using lipofectamine 2000 (Life Technology), according to the manufacturer's instructions.

Cytosolic and mitochondrial Ca^{2+} imaging

For cytosolic Ca^{2+}, cells were incubated with 4 µM of the Ca^{2+} indicator Fluo4-AM (Life Technology) in DMEM for 25 min at 37°C, washed three times with HT buffer [Hepes-Tris buffer (5.5 mM D-glucose, 132 mM NaCl, 4.2 mM KCl, 1 mM $CaCl_2$, 1 mM $MgCl_2$, and 10 mM HEPES pH 7.4)] and placed in a heated live-imaging station (lens, stage, and perfusion lines were maintained at 37°C). Alternatively, cells were transfected with the plasmid pGP-CMV-GCaMP6s (Addgene) expressing the cytosolic Ca^{2+} reporter. Live imaging was performed on a Leica TCS SP5 confocal microscope using a water-immersion 20× [0.7 NA] lens. During the recordings, cells were perfused with agents that induce release of intracellular Ca^{2+} stores (1 mM ATP, 1 µM bradikynin or 1 µM thapsigargin) in HT imaging buffer. Images were taken every 2 s.

For mitochondrial Ca^{2+}, MEFs were transfected with pTurbo-mitoGCaMP6. The GCaMP6 coding region was amplified from pGP-CMV-GCaMP6s, a N-terminal mitochondrial-targeting signal from the F_0 subunit C of ATPase was added, and the ligated product cloned into the *Age*I and *Not*I sites of the pTurbo vector (Evrogen).

Changes in fluorescent intensities over time were measured in individual cells after thresholding of the images using Metamorph. Individual data points were plotted as F/F0, and graphs obtained and statistical analyses performed by using the OriginPro software.

Immunocytochemistry

For immunocytochemistry, cells grown on glass coverslips were fixed with 4% paraformaldehyde (PFA; 10 min), followed by three washes in PBS at room temperature. The following primary antibodies were used: hemagglutinin (HA)-Tag (6E2) mouse monoclonal antibody (mAb) (Cell Signaling, 1:200, cat. no. 2367), TOM20 (FL-145) rabbit polyclonal IgG (Santa Cruz Biotechnology, 1:500, cat. no. sc-11415). Secondary Cy2 anti-mouse-IgG and Cy3 anti-rabbit-IgG antibodies (Jackson ImmunoResearch, 1:250, cat. no. 115-035-146 and 111-035-144, respectively) were used for fluorescence immunodetection.

Mitochondrial Ca^{2+} uptake

Mitochondrial Ca^{2+} uptake was estimated fluorometrically with the Ca^{2+}-sensitive fluorescent dye Calcium Green-5N (CG5N). Mitochondria (0.15−0.25 mg/ml) were added to 2 ml of incubation medium (125 mM KCl, 20 mM HEPES pH 7.2, 10 mM NaCl, 4 mM Na_2PO_4, 5 mM glutamate, 2.5 mM malate, 40 mM EGTA, 100 nM CG5N). Changes in fluorescence were recorded in an F-7000 spectrofluorometer (Hitachi) using 340/380 nm excitation and 510 nm emission wavelengths. Experiments were performed in a fluorimeter cuvette at 37°C. Bolus additions of Ca^{2+} (25 µM $CaCl_2$) were made to the mitochondrial suspension every 150 s, until mitochondria were unable to take up further Ca^{2+}. To correlate the CG5N fluorescence response to the Ca^{2+} concentration, consecutive Ca^{2+} additions of 40, 40, 20 nmol and, then, by 10 nmol were done, until Ca^{2+} was no longer accumulated.

ER-mitochondria colocalization

MEFs were transfected with Sec61-GFP (ER marker, green) and mito-Dsred (mitochondrial marker, red) using lipofectamine 2000. After 48 h, cells were fixed with 4% PFA for 10 min, followed by three washes in PBS. Z-stack images were obtained using a Leica TCS SP5 spectral confocal microscope. Ten random fields per coverslip were imaged and the colocalization of the two fluorochromes was assessed by the colocalization function in MetaMorph.

Statistical analyses

Data were expressed as the mean±s.e.m. Differences between two groups were evaluated by two-tailed, unpaired, Student's *t*-test, with significance set at $P<0.05$. Differences among multiple groups were evaluated by ANOVA with Tukey's correction; $*P<0.05$, $**P<0.01$, $***P<0.001$.

Acknowledgements

We thank Dr José M. Cuezva (Departmento de Biología Molecular Severo Ochoa, Universidad Autónoma de Madrid) for providing the anti-IF1 antibody.

Competing interests

The authors declare no competing or financial interests.

Author contributions

Conceptualization: F.V., A.G., A. Starkov, J.B., L.R.L., G.M.; Methodology: F.V., C.K., M.D'A., L.S.R.-E., A.G., J.M., J.B., L.R.L., G.M.; Formal analysis: F.V., C.K., M.D'A., L.S.R.-E., A. Stepanova, S.R.B., A. Starkov; Investigation: F.V., C.K., M.D'A., L.S.R.-E., A. Stepanova, S.R.B.; Resources: J.M., J.B., L.R.L., G.M.; Writing - original draft: F.V., J.B., L.R.L., G.M.; Project administration: G.M.; Funding acquisition: J.B., L.R.L., G.M.

Funding
This work was supported by the National Institutes of Health [R01GM088999 (to G.M.) and R01GM107442 (to L.R.L. and J.B.)]. Deposited in PMC for release after 12 months.

Supplementary information
Supplementary information available online at
http://jcs.biologists.org/lookup/doi/10.1242/jcs.206318.supplemental

References

Acin-Perez, R., Salazar, E., Brosel, S., Yang, H., Schon, E. A. and Manfredi, G. (2009a). Modulation of mitochondrial protein phosphorylation by soluble adenylyl cyclase ameliorates cytochrome oxidase defects. *EMBO Mol. Med.* **1**, 392-406.
Acin-Perez, R., Salazar, E., Kamenetsky, M., Buck, J., Levin, L. R. and Manfredi, G. (2009b). Cyclic AMP produced inside mitochondria regulates oxidative phosphorylation. *Cell Metab.* **9**, 265-276.
Area-Gomez, E., Del Carmen Lara Castillo, M., Tambini, M. D., Guardia-Laguarta, C., de Groof, A. J. C., Madra, M., Ikenouchi, J., Umeda, M., Bird, T. D., Sturley, S. L. et al. (2012). Upregulated function of mitochondria-associated ER membranes in Alzheimer disease. *EMBO J.* **31**, 4106-4123.
Birch-Machin, M. A. and Turnbull, D. M. (2001). Assaying mitochondrial respiratory complex activity in mitochondria isolated from human cells and tissues. *Methods Cell Biol.* **65**, 97-117.
Bitterman, J. L., Ramos-Espiritu, L., Diaz, A., Levin, L. R. and Buck, J. (2013). Pharmacological distinction between soluble and transmembrane adenylyl cyclases. *J. Pharmacol. Exp. Ther.* **347**, 589-598.
Bundey, R. A. and Insel, P. A. (2004). Discrete intracellular signaling domains of soluble adenylyl cyclase: camps of cAMP? *Sci. STKE* **2004**, e19.
Buxton, I. L. and Brunton, L. L. (1983). Compartments of cyclic AMP and protein kinase in mammalian cardiomyocytes. *J. Biol. Chem.* **258**, 10233-10239.
Buxton, I. L. O. and Brunton, L. L. (1986). Compartmentation of hormone action in adult mammalian cardiomyocytes. *Adv. Exp. Med. Biol.* **194**, 117-127.
Cárdenas, C., Miller, R. A., Smith, I., Bui, T., Molgó, J., Müller, M., Vais, H., Cheung, K.-H., Yang, J., Parker, I. et al. (2010). Essential regulation of cell bioenergetics by constitutive InsP3 receptor Ca2+ transfer to mitochondria. *Cell* **142**, 270-283.
Chen, T.-W., Wardill, T. J., Sun, Y., Pulver, S. R., Renninger, S. L., Baohan, A., Schreiter, E. R., Kerr, R. A., Orger, M. B., Jayaraman, V. et al. (2013). Ultrasensitive fluorescent proteins for imaging neuronal activity. *Nature* **499**, 295-300.
Davare, M. A., Avdonin, V., Hall, D. D., Peden, E. M., Burette, A., Weinberg, R. J., Horne, M. C., Hoshi, T. and Hell, J. W. (2001). A beta2 adrenergic receptor signaling complex assembled with the Ca2+ channel Cav1.2. *Science* **293**, 98-101.
De Rasmo, D., Signorile, A., Santeramo, A., Larizza, M., Lattanzio, P., Capitanio, G. and Papa, S. (2015). Intramitochondrial adenylyl cyclase controls the turnover of nuclear-encoded subunits and activity of mammalian complex I of the respiratory chain. *Biochim. Biophys. Acta* **1853**, 183-191.
De Stefani, D., Patron, M. and Rizzuto, R. (2015). Structure and function of the mitochondrial calcium uniporter complex. *Biochim. Biophys. Acta* **1853**, 2006-2011.
Denton, R. M. (2009). Regulation of mitochondrial dehydrogenases by calcium ions. *Biochim. Biophys. Acta* **1787**, 1309-1316.
Di Benedetto, G., Scalzotto, E., Mongillo, M. and Pozzan, T. (2013). Mitochondrial Ca(2)(+) uptake induces cyclic AMP generation in the matrix and modulates organelle ATP levels. *Cell Metab.* **17**, 965-975.
Di Benedetto, G., Pendin, D., Greotti, E., Pizzo, P. and Pozzan, T. (2014). Ca2+ and cAMP cross-talk in mitochondria. *J. Physiol.* **592**, 305-312.
Distelmaier, F., Valsecchi, F., Forkink, M., van Emst-de Vries, S., Swarts, H. G., Rodenburg, R. J. T., Verwiel, E. T. P., Smeitink, J. A. M., Willems, P. H. G. M. and Koopman, W. J. H. (2012). Trolox-sensitive reactive oxygen species regulate mitochondrial morphology, oxidative phosphorylation and cytosolic calcium handling in healthy cells. *Antioxid Redox Signal.* **17**, 1657-1669.
Ferris, C. D., Cameron, A. M., Bredt, D. S., Huganir, R. L. and Snyder, S. H. (1991). Inositol 1,4,5-trisphosphate receptor is phosphorylated by cyclic AMP-dependent protein kinase at serines 1755 and 1589. *Biochem. Biophys. Res. Commun.* **175**, 192-198.
García-Bermúdez, J., Sánchez-Aragó, M., Soldevilla, B., Del Arco, A., Nuevo-Tapioles, C. and Cuezva, J. M. (2015). PKA phosphorylates the ATPase inhibitory factor 1 and inactivates its capacity to bind and inhibit the mitochondrial H(+)-ATP synthase. *Cell Rep.* **12**, 2143-2155.
Han, Y., Wang, Q., Song, P., Zhu, Y. and Zou, M.-H. (2010). Redox regulation of the AMP-activated protein kinase. *PLoS ONE* **5**, e15420.
Hardie, D. G. (2007). AMP-activated/SNF1 protein kinases: conserved guardians of cellular energy. *Nat. Rev. Mol. Cell Biol.* **8**, 774-785.
Hardie, D. G., Ross, F. A. and Hawley, S. A. (2012). AMPK: a nutrient and energy sensor that maintains energy homeostasis. *Nat. Rev. Mol. Cell Biol.* **13**, 251-262.
Hawley, S. A., Ross, F. A., Chevtzoff, C., Green, K. A., Evans, A., Fogarty, S., Towler, M. C., Brown, L. J., Ogunbayo, O. A., Evans, A. M. et al. (2010). Use of cells expressing gamma subunit variants to identify diverse mechanisms of AMPK activation. *Cell Metab.* **11**, 554-565.
Hayashi, T., Rizzuto, R., Hajnoczky, G. and Su, T.-P. (2009). MAM: more than just a housekeeper. *Trends Cell Biol.* **19**, 81-88.
Hess, K. C., Liu, J., Manfredi, G., Muhlschlegel, F. A., Buck, J., Levin, L. R. and Barrientos, A. (2014). A mitochondrial CO2-adenylyl cyclase-cAMP signalosome controls yeast normoxic cytochrome c oxidase activity. *FASEB J.* **28**, 4369-4380.
Inda, C., Dos Santos Claro, P. A., Bonfiglio, J. J., Senin, S. A., Maccarrone, G., Turck, C. W. and Silberstein, S. (2016). Different cAMP sources are critically involved in G protein-coupled receptor CRHR1 signaling. *J. Cell Biol.* **214**, 181-195.
Kamer, K. J. and Mootha, V. K. (2015). The molecular era of the mitochondrial calcium uniporter. *Nat. Rev. Mol. Cell Biol.* **16**, 545-553.
Koopman, W. J. H., Visch, H.-J., Verkaart, S., van den Heuvel, L. W. P. J., Smeitink, J. A. M. and Willems, P. H. G. M. (2005). Mitochondrial network complexity and pathological decrease in complex I activity are tightly correlated in isolated human complex I deficiency. *Am. J. Physiol. Cell Physiol.* **289**, C881-C890.
Koopman, W. J. H., Verkaart, S., van Emst-de Vries, S. E., Grefte, S., Smeitink, J. A. M. and Willems, P. H. G. M. (2006). Simultaneous quantification of oxidative stress and cell spreading using 5-(and-6)-chloromethyl-2′,7′-dichlorofluorescein. *Cytometry A* **69**, 1184-1192.
Lefkimmiatis, K. and Zaccolo, M. (2014). cAMP signaling in subcellular compartments. *Pharmacol. Ther.* **143**, 295-304.
Lefkimmiatis, K., Leronni, D. and Hofer, A. M. (2013). The inner and outer compartments of mitochondria are sites of distinct cAMP/PKA signaling dynamics. *J. Cell Biol.* **202**, 453-462.
Marx, S. O., Kurokawa, J., Reiken, S., Motoike, H., D'Armiento, J., Marks, A. R. and Kass, R. S. (2002). Requirement of a macromolecular signaling complex for beta adrenergic receptor modulation of the KCNQ1-KCNE1 potassium channel. *Science* **295**, 496-499.
Monterisi, S. and Zaccolo, M. (2017). Components of the mitochondrial cAMP signalosome. *Biochem. Soc. Trans.* **45**, 269-274.
Monterisi, S., Lobo, M. J., Livie, C., Castle, J. C., Weinberger, M., Baillie, G. S., Surdo, N. C., Musheshe, N., Stangherlin, A., Gottlieb, E. et al. (2017). PDE2A2 regulates mitochondria morphology and apoptotic cell death via local modulation of cAMP/PKA signalling. *Elife* **6**, e21374.
Nakade, S., Rhee, S. K., Hamanaka, H. and Mikoshiba, K. (1994). Cyclic AMP-dependent phosphorylation of an immunoaffinity-purified homotetrameric inositol 1,4,5-trisphosphate receptor (type I) increases Ca2+ flux in reconstituted lipid vesicles. *J. Biol. Chem.* **269**, 6735-6742.
Oakes, S. A., Scorrano, L., Opferman, J. T., Bassik, M. C., Nishino, M., Pozzan, T. and Korsmeyer, S. J. (2005). Proapoptotic BAX and BAK regulate the type 1 inositol trisphosphate receptor and calcium leak from the endoplasmic reticulum. *Proc. Natl. Acad. Sci. USA* **102**, 105-110.
Rahman, N., Ramos-Espiritu, L., Milner, T. A., Buck, J. and Levin, L. R. (2016). Soluble adenylyl cyclase is essential for proper lysosomal acidification. *J. Gen. Physiol.* **148**, 325-339.
Ramos-Espiritu, L., Diaz, A., Nardin, C., Saviola, A. J., Shaw, F., Plitt, T., Yang, X., Wolchok, J., Pirog, E. C., Desman, G. et al. (2016a). The metabolic/pH sensor soluble adenylyl cyclase is a tumor suppressor protein. *Oncotarget* **7**, 45597-45607.
Ramos-Espiritu, L., Kleinboelting, S., Navarrete, F. A., Alvau, A., Visconti, P. E., Valsecchi, F., Starkov, A., Manfredi, G., Buck, H., Adura, C. et al. (2016b). Discovery of LRE1 as a specific and allosteric inhibitor of soluble adenylyl cyclase. *Nat. Chem. Biol.* **12**, 838-844.
Reiken, S., Lacampagne, A., Zhou, H., Kherani, A., Lehnart, S. E., Ward, C., Huang, F., Gaburjakova, M., Gaburjakova, J., Rosemblit, N. et al. (2003). PKA phosphorylation activates the calcium release channel (ryanodine receptor) in skeletal muscle: defective regulation in heart failure. *J. Cell Biol.* **160**, 919-928.
Robinson, B. H. (1996). Use of fibroblast and lymphoblast cultures for detection of respiratory chain defects. *Methods Enzymol.* **264**, 454-464.
Ruderman, N. B., Xu, X. J., Nelson, L., Cacicedo, J. M., Saha, A. K., Lan, F. and Ido, Y. (2010). AMPK and SIRT1: a long-standing partnership? *Am. J. Physiol. Endocrinol. Metab.* **298**, E751-E760.
Satrustegui, J., Pardo, B. and Del Arco, A. (2007). Mitochondrial transporters as novel targets for intracellular calcium signaling. *Physiol. Rev.* **87**, 29-67.
Scarpulla, R. C. (2011). Metabolic control of mitochondrial biogenesis through the PGC-1 family regulatory network. *Biochim. Biophys. Acta* **1813**, 1269-1278.
Scarpulla, R. C. (2012). Nucleus-encoded regulators of mitochondrial function: integration of respiratory chain expression, nutrient sensing and metabolic stress. *Biochim. Biophys. Acta* **1819**, 1088-1097.
Shaywitz, A. J. and Greenberg, M. E. (1999). CREB: a stimulus-induced transcription factor activated by a diverse array of extracellular signals. *Annu. Rev. Biochem.* **68**, 821-861.
Szabadkai, G. and Rizzuto, R. (2004). Participation of endoplasmic reticulum and mitochondrial calcium handling in apoptosis: more than just neighborhood? *FEBS Lett.* **567**, 111-115.

Tang, T. S., Tu, H., Wang, Z. and Bezprozvanny, I. (2003). Modulation of type 1 inositol (1,4,5)-trisphosphate receptor function by protein kinase a and protein phosphatase 1alpha. *J. Neurosci.* **23**, 403-415.

Valsecchi, F., Monge, C., Forkink, M., de Groof, A. J., Benard, G., Rossignol, R., Swarts, H. G., van Emst-de Vries, S. E., Rodenburg, R. J., Calvaruso, M. A. et al. (2012). Metabolic consequences of NDUFS4 gene deletion in immortalized mouse embryonic fibroblasts. *Biochim. Biophys. Acta*.

Valsecchi, F., Ramos-Espiritu, L. S., Buck, J., Levin, L. R. and Manfredi, G. (2013). cAMP and mitochondria. *Physiology (Bethesda)* **28**, 199-209.

Valsecchi, F., Konrad, C. and Manfredi, G. (2014). Role of soluble adenylyl cyclase in mitochondria. *Biochim. Biophys. Acta* **1842**, 2555-2560.

Vanderheyden, V., Devogelaere, B., Missiaen, L., De Smedt, H., Bultynck, G. and Parys, J. B. (2009). Regulation of inositol 1,4,5-trisphosphate-induced Ca2+ release by reversible phosphorylation and dephosphorylation. *Biochim. Biophys. Acta* **1793**, 959-970.

Vives-Bauza, C., Yang, L. and Manfredi, G. (2007). Assay of mitochondrial ATP synthesis in animal cells and tissues. *Methods Cell Biol.* **80**, 155-171.

Wagner, L. E., II, Li, W.-H., Joseph, S. K. and Yule, D. I. (2004). Functional consequences of phosphomimetic mutations at key cAMP-dependent protein kinase phosphorylation sites in the type 1 inositol 1,4,5-trisphosphate receptor. *J. Biol. Chem.* **279**, 46242-46252.

Wang, Z., Liu, D., Varin, A., Nicolas, V., Courilleau, D., Mateo, P., Caubere, C., Rouet, P., Gomez, A.-M., Vandecasteele, G. et al. (2016). A cardiac mitochondrial cAMP signaling pathway regulates calcium accumulation, permeability transition and cell death. *Cell Death Dis.* **7**, e2198.

Witczak, C. A., Sharoff, C. G. and Goodyear, L. J. (2008). AMP-activated protein kinase in skeletal muscle: from structure and localization to its role as a master regulator of cellular metabolism. *Cell. Mol. Life Sci.* **65**, 3737-3755.

Zippin, J. H., Chen, Y., Nahirney, P., Kamenetsky, M., Wuttke, M. S., Fischman, D. A., Levin, L. R. and Buck, J. (2003). Compartmentalization of bicarbonate-sensitive adenylyl cyclase in distinct signaling microdomains. *FASEB J.* **17**, 82-84.

Zmijewski, J. W., Banerjee, S., Bae, H., Friggeri, A., Lazarowski, E. R. and Abraham, E. (2010). Exposure to hydrogen peroxide induces oxidation and activation of AMP-activated protein kinase. *J. Biol. Chem.* **285**, 33154-33164.

Valsecchi Supplementary Figure 1

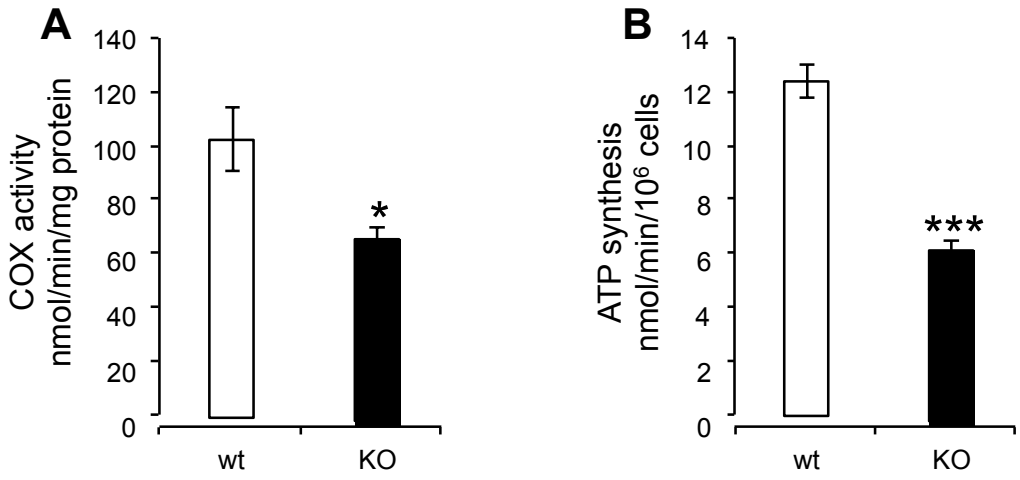

Figure S1: COX activity and ATP synthesis in wt2 and sAC KO2 MEFs

A) COX activity in independent lines of wt2 and sAC KO2 MEFs (n=3). B) ATP synthesis in permeabilized wt2 and sAC KO2 MEFs (n=3). Data is expressed as mean±s.e.m. in indicated number of different biological replicates (*p<0.05, ***p<0.001, Student's *t*-test).

Valsecchi Supplementary Figure 2

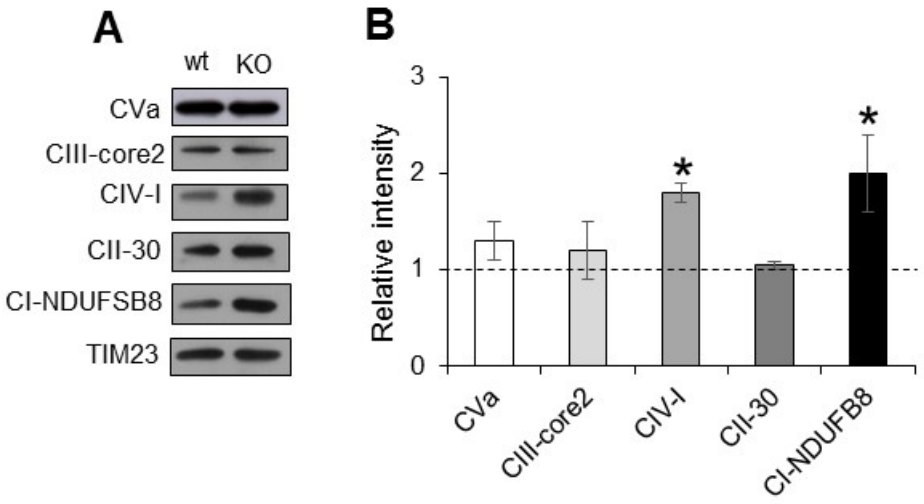

Figure S2: Quantification of OXPHOS proteins in isolated mitochondria from wt and sAC KO cells.

A) Representative western blot of OXPHOS subunits and TIM23. B) Quantification of band intensity normalized by TIM23 (n=5). Data is expressed as mean±s.e.m. in indicated number of different biological replicates (*p<0.05, Student's *t*-test).

Valsecchi Supplementary Figure 3

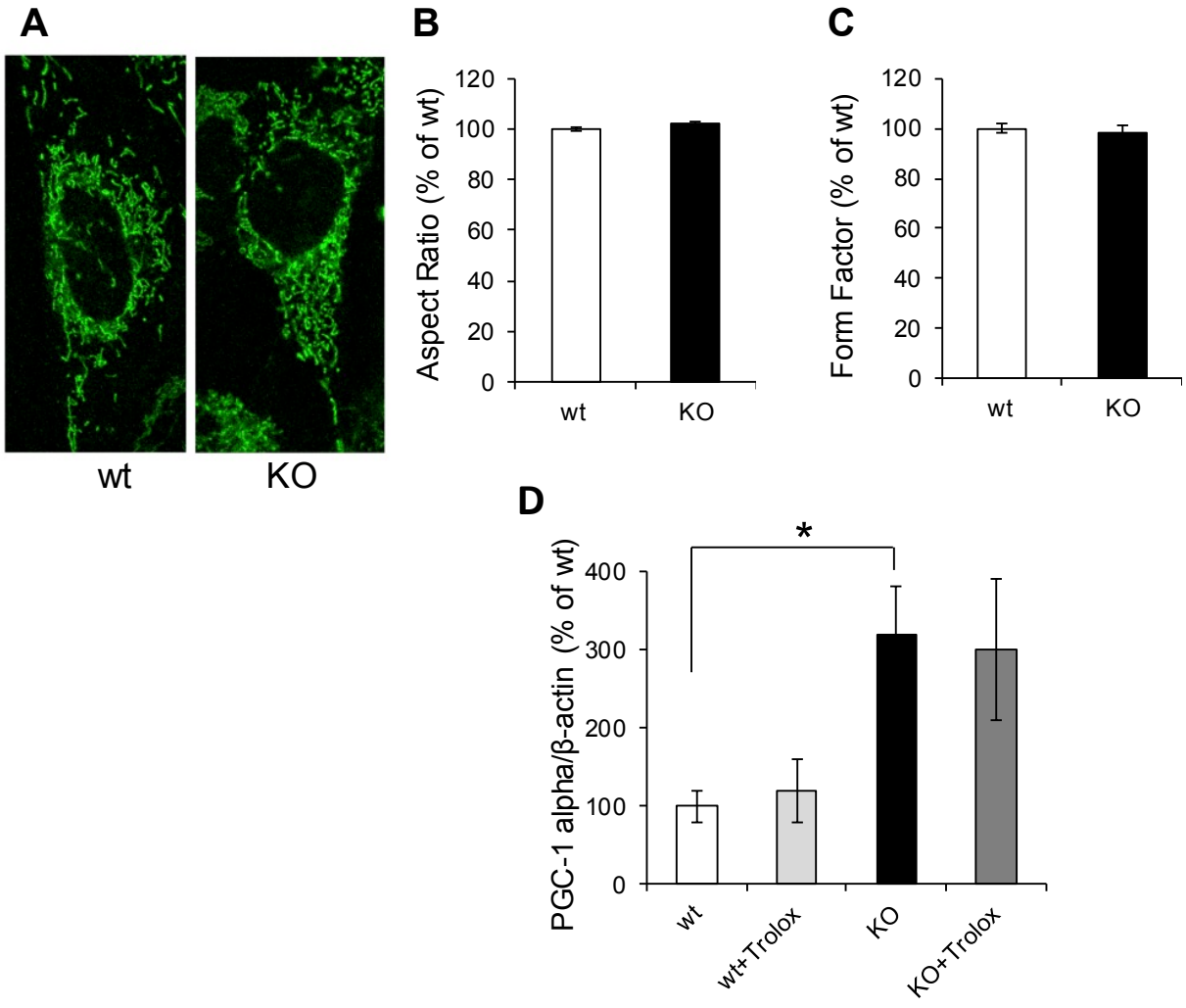

Figure S3: mitochondrial morphology and effect of antioxidants on PGC-1α expression. A) Representative image of wt and sAC KO cells loaded with MitoTracker Green 50nM. B) Mitochondria aspect ratio in wt and sAC KO MEFs expressed as % of wt. C) Mitochondrial form factor in wt and sAC KO MEFs expressed as a % of wt. In B and C, n=48-83 in 3 experiments. D) Effects of the antioxidant Trolox on PGC-1α mRNA content (n=3) in wt and sAc KO cells. Data is expressed as mean±s.e.m. in indicated number of different biological replicates (*$p<0.05$, ANOVA with Tukey's correction).

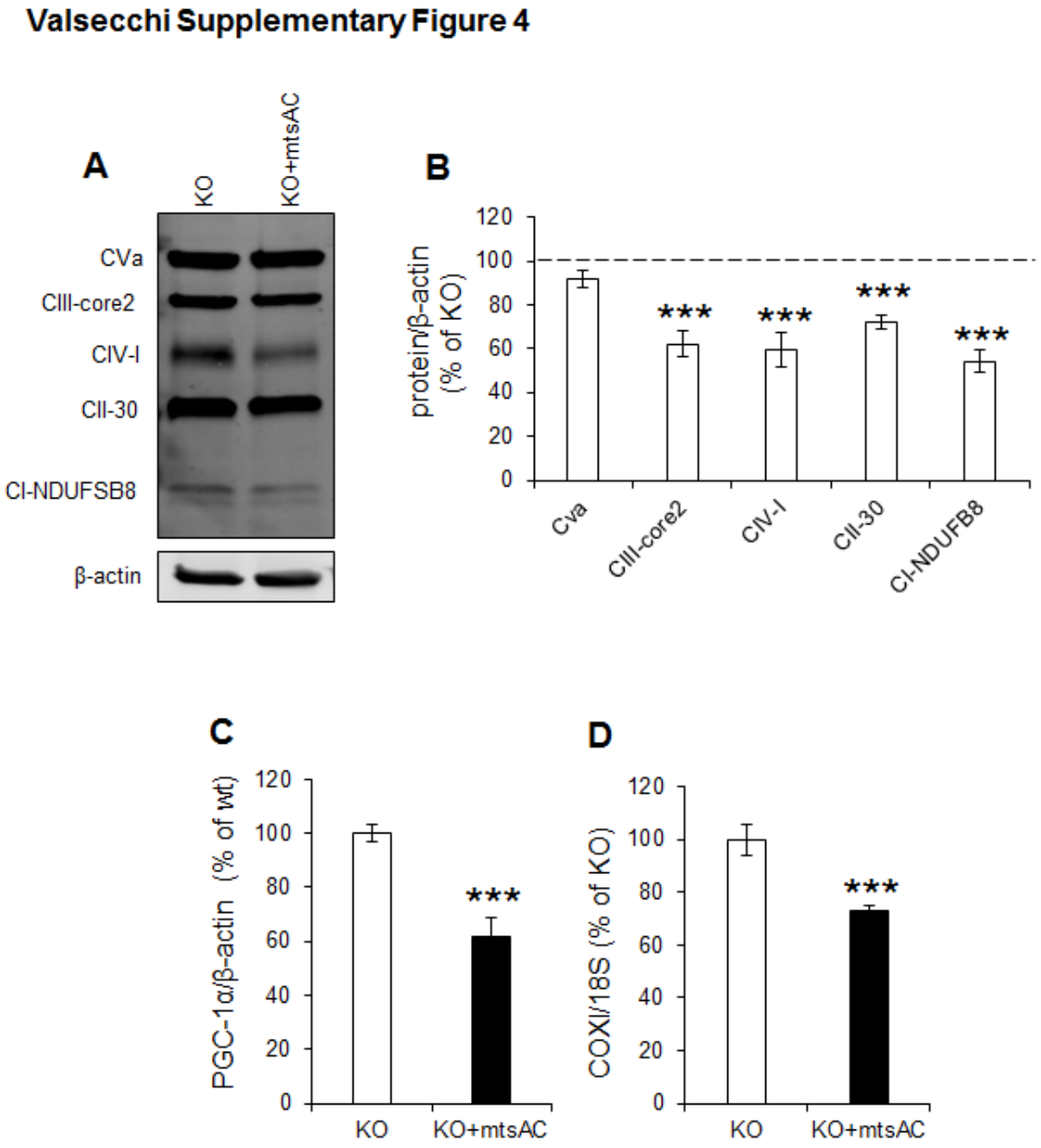

Figure S4: mtsAC expression decreases OXPHOS component content in KO cells. A) representative western blot of KO and KO+mtsAC cells probed with OXPHOS cocktails antibody. B) Quantification of the western blot. C) mRNA level of PGC1α expressed as % of KO. C) Mitochondrial DNA content expressed as % of KO (COXI gene normalized by 18S rRNA). Data is expressed as mean±s.e.m. in indicated number of different biological replicates (***p<0.001, Student's *t*-test).

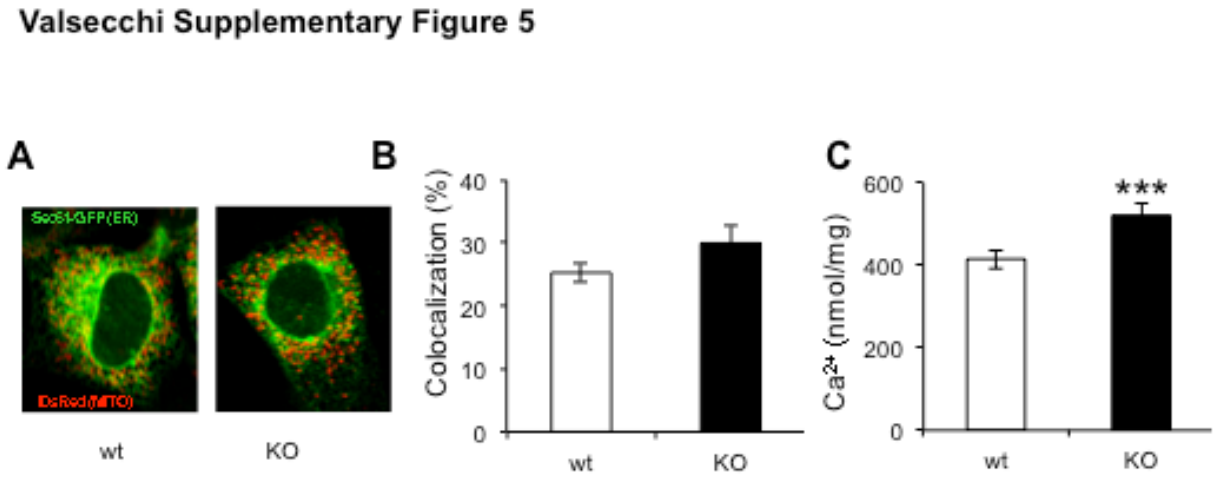

Figure S5: mitochondria Ca^{2+} uptake and ER-mitochondria colocalization

A) Representative images of wt and sAC KO cells co-transfected with the ER protein Sec61-GFP (green) and mitochondrial mitoDsRed (red). B) Quantification of ER-Sec61-GFP and mitoDsRed colocalization assessed by the co-localization function of MetaMorph expresses as % of red over green. C) Mitochondrial Ca^{2+} uptake in isolated mitochondria from wt and sAC KO MEFs (n=3). Data is expressed as mean±s.e.m. in indicated number of different biological replicates (***$p<0.001$, Student's *t*-test).

Valsecchi Supplementary Figure 6

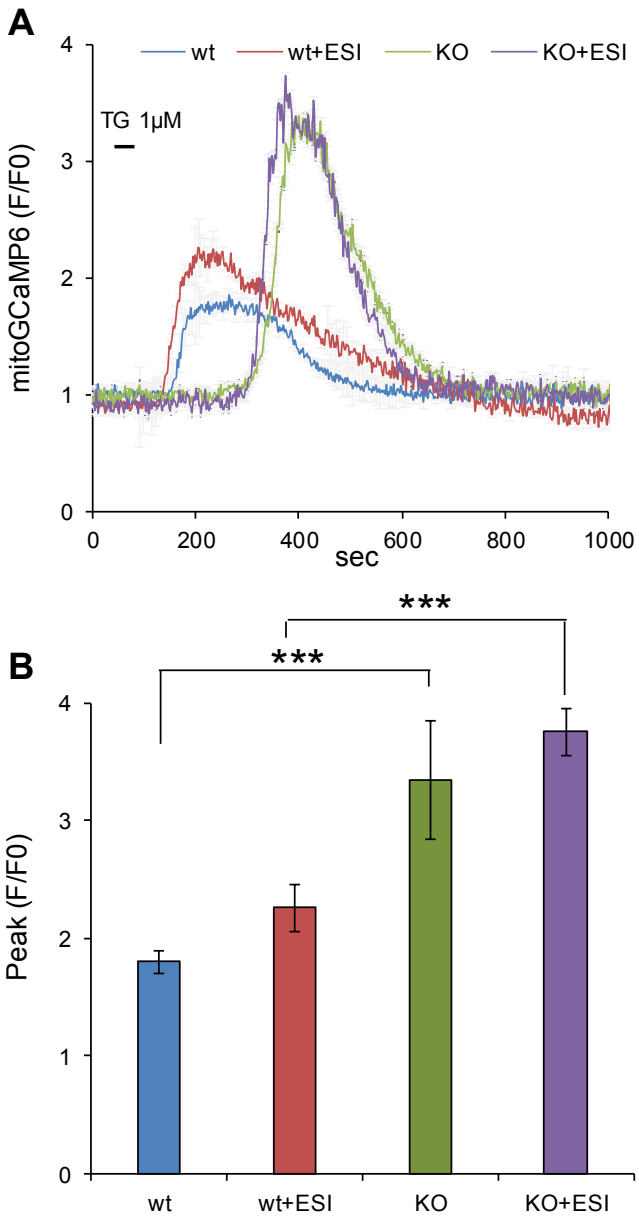

Figure S6: Effect of EPAC inhibitor ESI-09 on mitochondrial Ca^{2+} uptake A) Fluorescent traces of mitoGCaMP6 in wt and sAC KO (KO) MEFs treated with and without ESI-09 (ESI) and stimulated with TG. B) Quantification of mitoGCaMP6 fluorescence peaks (n=40, 32, 28, and 44 cells, for wt, wt + ESI, sAC KO, and sAC KO + ESI, respectively). Data is expressed as mean±s.e.m. in indicated number of different biological replicates (***p<0.001, ANOVA with Tukey's correction).

Valsecchi Supplementary Figure 7

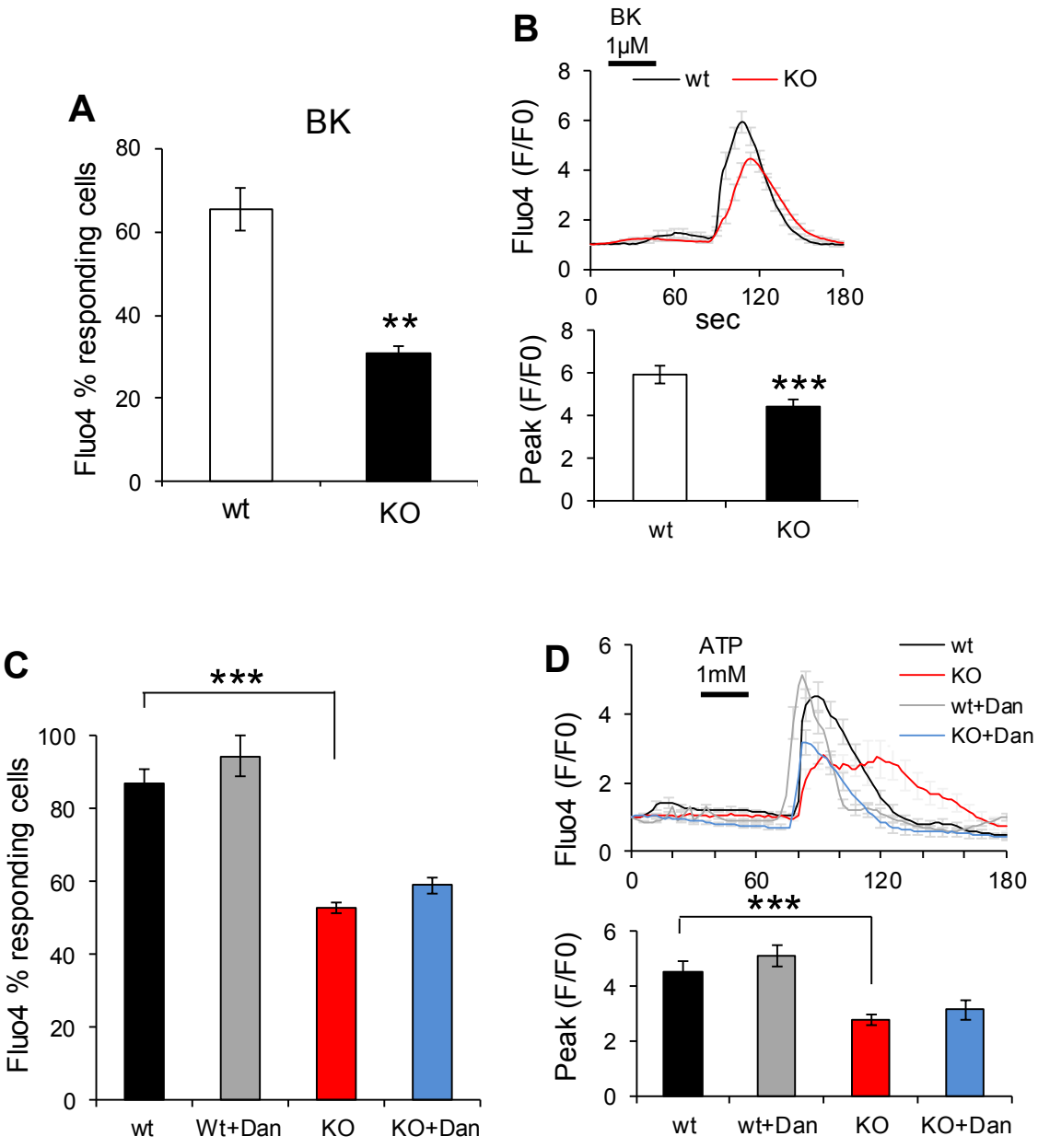

Figure S7: cytosolic ER Ca^{2+} release induced by Bradykinin stimulation, effects of dantrolene on ER Ca^{2+} release,

A) Percentage of responding wt and sAC KO MEFs upon Bradykinin (BK) stimulation. B) Top panel: Average fluo4 fluorescence curve in wt and sAC KO cells stimulated with 1µM bradykinin; Bottom panel: quantification of Ca^{2+} peak in responding wt and sAC KO cells

(n=33-66 cells, in 3 independent experiments). Data is expressed as mean±s.e.m. in indicated number of different biological replicates (**p<0.01, ***p<0.001, Student's *t*-test). C) Percentage of responding wt and sAC KO cells with and without dantrolene (10µM for 1 hour pre-incubation and in the perfusion buffer) and ATP (1mM). D) Top panel: fluo4 fluorescence in wt and sAC KO cells stimulated with ATP (1mM) in the presence or absence of dantrolene. Bottom Panel: quantification of the Fluo4 peak intensity in cells stimulated by ATP with and without dantrolene (n=15-27 cells, in 3 independent experiments). Data is expressed as mean±s.e.m. in indicated number of different biological replicates (***p<0.001, ANOVA with Tukey's correction).

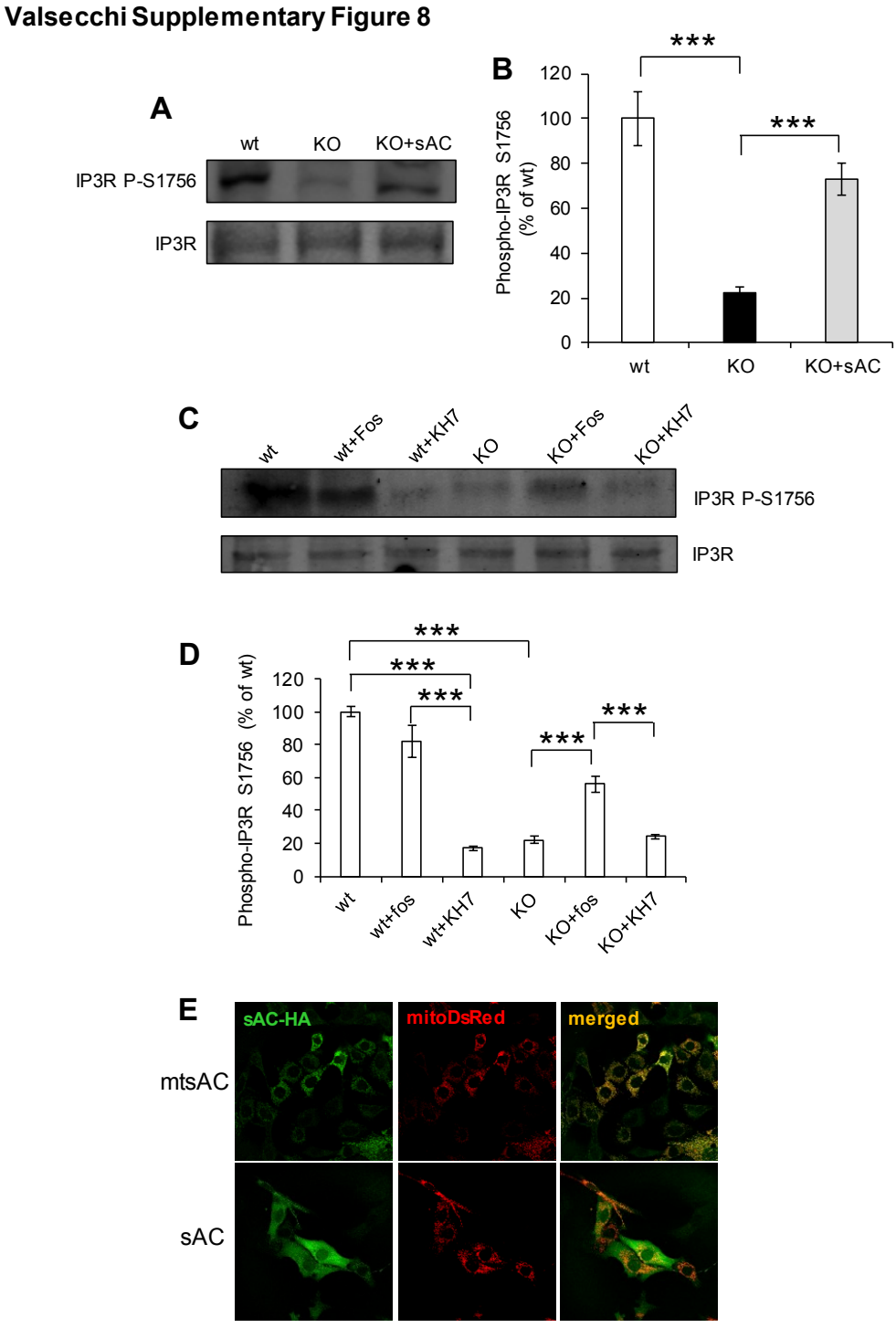

Figure S8: IP3R phosphorylation is regulated by sAC by forskolin or KH7.

A) Representative western blot of IP3R P-S1756 and total IP3R in wt, KO and KO+sAC cells. B) Quantification of P-S1756 normalized by total IP3R, in KO and KO+sAC cells expressed as % of wt (n=3). C) Representative western blot of IP3R P-S1756 and total IP3R in wt, and KO cells treated with forskolin and KH7. D) Quantification of P-S1756 normalized by total IP3R, in KO and KO+sAC cells expressed as % of wt (n=3). Data is expressed as mean±s.e.m. in

indicated number of different biological replicates (***$p<0.001$, ANOVA with Tukey's correction). E) Representative images of MEF cells co-transfected with mtsAC-HA or sAC-HA (green) and mitoDsRed (red) and merged images.